THE ASTROPHYSICAL JOURNAL, 271:89–112, 1983 August 1

COMPTON HEATED WINDS AND CORONAE ABOVE ACCRETION DISKS. II. RADIATIVE TRANSFER AND OBSERVABLE CONSEQUENCES

MITCHELL C. BEGELMAN[1,3] AND CHRISTOPHER F. MCKEE[1,2]
Received 1982 June 24; accepted 1983 January 21

ABSTRACT

In another paper (Paper I), we analyzed the dynamics of winds driven from accretion disks when the outer regions are irradiated by X-rays from the inner regions. The observable manifestations of Compton heated coronae and winds may depend sensitively on the transfer of incident X-rays through the corona and wind. Here we incorporate, into the framework laid down in Paper I, the effects of attenuation and scattering on X-rays from a central source, as well as the effects of inverse Compton cooling due to radiation emitted locally by the disk.

The observable signatures of Compton heated winds and coronae above accretion disks in quasars, active galactic nuclei, X-ray binaries, and cataclysmic variables include: (1) an extended source of scattered X-rays, able to account in detail for the partial X-ray eclipses of sources such as 4U 2129+47 and 4U 1822−37; (2) X-ray polarization at a level ranging from more than 1% for a typical source with random orientation to more than ~10% for a nearly edge-on source with the compact X-ray source obscured; (3) line emission due to reprocessing of incident X-rays by the disk, with an efficiency which decreases as the X-ray flux increases (4U 1822−37 is treated as an example); and (4) reprocessed continuum with a spectrum which often differs from the scaling $F_\nu \propto \nu^{1/3}$ predicted for continuum generated locally within the disk; the results are applied to the UV spectrum of Cyg X-2.

Subject headings: galaxies: Seyfert — quasars — stars: accretion — X-rays: binaries

I. INTRODUCTION

In another paper (Begelman, McKee, and Shields 1983 [Paper I]), we showed that a strong wind can arise when the outer part of an accretion disk is irradiated by X-rays from the central regions. The wind occurs outside a radius $\sim 0.1 R_{IC}$, where R_{IC} is the radius at which the free-fall velocity equals the isothermal sound speed of the Compton-heated coronal gas (see eq. [2.1] in Paper I, denoted [I2.1]). We asserted that the asymptotic speed of the wind depends on radius, but is insensitive to radiative transfer effects which occur as the X-rays traverse the corona and wind. The transition between a strong wind at large radii and a tightly bound corona farther in is likewise insensitive to the effects of scattering, since the location of the transition depends on the spectrum of the incident radiation but not on its intensity. We argued, therefore, that the mass loss rate at each point in the disk should be affected by radiative transfer only insofar as attenuation reduces the intensity and hence the pressure at the base of the flow. We expressed this reduction through an "attenuation factor" f, defined as the ratio of the actual mean intensity at the base of the flow to the unattenuated intensity. We asserted that f would exceed 0.1 in the wind zone.

Our aim in this paper is first to verify that the above assertions are correct, and second, to explore the important observable effects of Compton-heated gas above an accretion disk. Evidence for extended sources of scattered X-rays in partially eclipsing X-ray binaries has already motivated research into the properties of Compton-heated coronae above disks by White and Holt (1982); McClintock *et al.* (1982); and Fabian, Guilbert, and Ross (1982). Scattering, particularly by the flattened distributions of gas in the corona, can give rise to substantial linear polarization. Some of the X-ray energy not used to heat the corona/wind will be absorbed by the underlying disk, and converted into emission lines and/or a flux in continuum which can swamp the emission intrinsic to the disk.

These "directly observable" manifestations of Compton heated winds and coronae are more closely intertwined with radiative transfer effects than are the dynamical consequences emphasized in Paper I. For a disk irradiated at a low angle of incidence by a central X-ray source, the degree of attenuation in the corona/wind increases with *decreasing* radius, and with decreasing height above the disk. Although most of the heating which drives the wind occurs at larger radii and at heights $h \sim R$, the scattering which produces the observable effects may be dominated by the structure of the flow in these denser regions. To map the effects of scattering self-consistently, one must at least determine the attenuation factor f as a function of radius. The result depends sensitively on the geometric

[1] Astronomy Department, University of California, Berkeley.
[2] Physics Department, University of California, Berkeley.
[3] Institute of Astronomy, Cambridge, England.

arrangement of disk and source, and our attempt in § II to solve the problem for a steadily flaring (i.e., disk height h_d increasing at a rate faster than one proportional to R) disk irradiated by a central point source, represents the configuration in which radiative transfer effects are likely to be most important. They are indeed dramatic, particularly in the inner corona where the attenuation can become sufficiently great that the radiation emitted locally by the disk plays an important role in determining the thermal state of the gas. Attenuation of radiation from the source passing through the inner corona affects in turn the structure of the flow farther out. By incorporating these effects into the analysis of Paper I, we produce a model for the spatial structure of the corona/wind above a flaring disk. This model is summarized in Figure 1.

Once the attenuation factor is known, it is straightforward to describe the scattering, polarization, and reprocessing of X-rays by the disk, in detail. This is done in §§ III–V, where we emphasize applications to X-ray binaries, quasars, and Seyfert galaxies. In particular, we deduce a specific model for the partially eclipsing X-ray binary 4U 2129+47, which fits the available data as well as the more phenomenological treatment by McClintock *et al.* (1982).

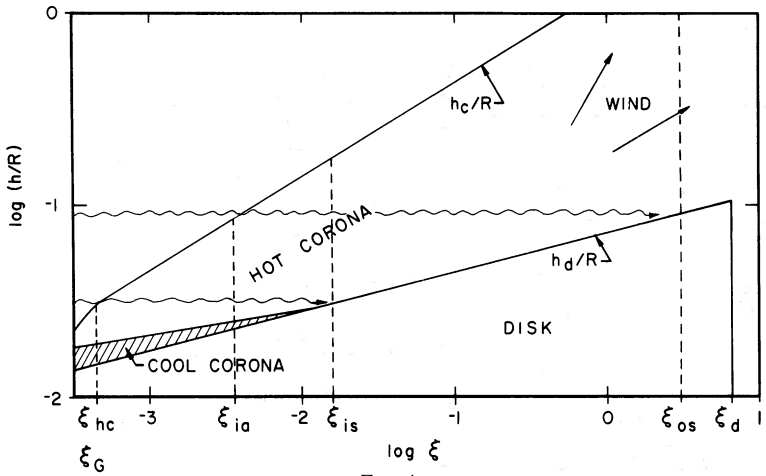

FIG. 1*a*

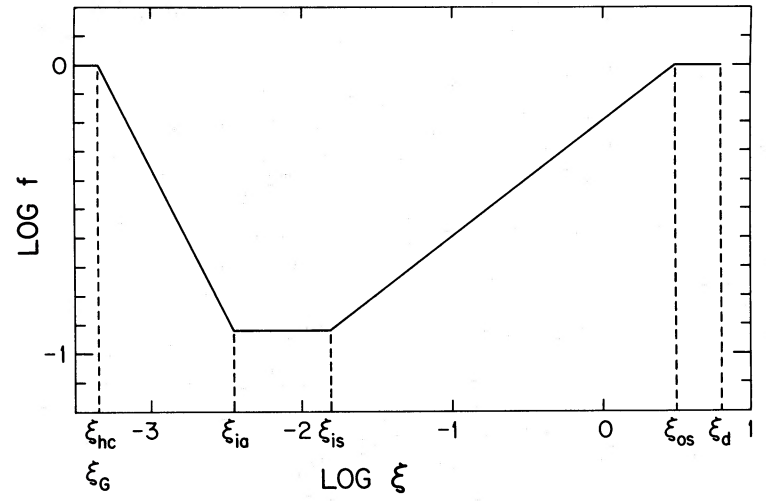

FIG. 1*b*

FIG. 1*a*.—Radiative transfer in the corona and wind. The normalized height of the surface of the disk h_d/R_0 and of the corona h_c/R_0 are plotted as functions of $\xi = R_0/R_{IC}$. Photons from the central source propagate horizontally in this figure; two examples are indicated by wavy lines. The case illustrated corresponds to $L = L_{cr}$ and $h_d/R = 0.07\xi^{0.2}$; also, $\epsilon_{-1} = T_{IC8} = \Xi'_{h,min} = k_\tau = 1$. For this choice of parameters, the point at which the corona becomes thicker than the disk ξ_G is the same as the point ξ_{hc} at which the local disk radiation is weak enough for the hot corona to exist (i.e., $T_h > T_{IC}/2$). In the inner attenuation zone ($\xi_{hc} < \xi < \xi_{ia}$) the hot corona is governed by the condition that the attenuation factor f equal f_d (eq. [4.11]). In the inner shadowed zone ($\xi_{ia} < \xi < \xi_{is}$), the hot corona has $\Xi'_0 = \Xi'_{h,min}$ and f is determined by absorption at $\xi < \xi_{ia}$. We have not analyzed the structure of the transition zone (the "cool corona") between the hot corona and the surface of the disk, but it is probably very opaque to photons from the central source. In the outer shadowed zone ($\xi_{is} < \xi < \xi_{os}$) the radiation from the central source can reach the surface of the disk, but f is still determined by attenuation at $\xi < \xi_{ia}$. Finally, in the outer attenuation zone ($\xi_{os} < \xi < \xi_d$) radiation from the central source passes above the inner attenuation zone and f is determined by local attenuation. The disk terminates at ξ_d.

FIG. 1*b*.—Attenuation factor $f(\xi)$ for disk illustrated in Fig. 1*a*. The minimum value of $f(\xi)$ is f_{is}, which is given by eq. (2.24) and is approximately 0.1 for the parameters adopted here.

II. RADIATIVE TRANSFER IN THE CORONA AND WIND

As we showed in Paper I (cf. eqs. [3.58] ff.), the mass flux in a given flow regime scales with the pressure p_0 at the base of the flow. The pressure, in turn, is proportional to the mean radiation intensity J_0 at the base of the flow (eq. [I2.1]); hence, it is important to compute this quantity self-consistently, taking into account the attenuation of the radiation as it passes through the hot gas. If the optical depth from the base of the flow to the source of radiation (τ_{s0}) is small, then the heating rate Γ is given by equation (I2.5) and the form factor for heating $f_\Gamma(y)$ (eq. [I3.9]) varies slowly between $y = 1$ and $y \sim 2$. However, if τ_{s0} exceeds unity, the intensity will be reduced below $L/4\pi R^2$, and the mass flux diminished. In this section we shall estimate the "attenuation factor"

$$f_{\Gamma_0} \equiv f \equiv \frac{4\pi J_0}{L/4\pi R_0^2} < 1 \tag{2.1}$$

as a function of the radius R_0 at the base of the flow, under the assumption that the optical depth is due to electron scattering. In terms of f, the pressure p_0 is

$$p_0 = \frac{Lf}{4\pi R_0^2 \Xi_0'}, \tag{2.2}$$

where $\Xi_0' = 4\pi J_0/p_0 c$ is evaluated at the base of the flow. In the wind $\Xi_0' = \Xi_{c,\max}'$ (see discussion after eq. [I2.1]), whereas in the corona a range of values is possible (see below).

Radiative transfer effects clearly depend on the geometry of the source and of the disk. Since the disk itself is assumed to be opaque, direct radiation from a central source can reach the base of the flow only if the source is larger than the thickness of the disk or if the disk flares—i.e., if the height of the disk photosphere $h_d(R_0)$ increases with R_0 faster than linearly. The structure of accretion disks is poorly known because of uncertainties in the viscosity, because of the possibility of nonviscous angular momentum transport (Blandford and Payne 1982), and, in the case of massive accretion disks, because of the complicating effects of self-gravity (e.g., Paczyński 1978). Standard thin disk models which parameterize the viscous stress as $\alpha_d p$ and which ignore the latter two effects do allow radiation from the central source to reach the disk (Shakura and Sunyaev 1973). The inner part of the disk is dominated by radiation pressure with the opacity due to electron scattering; it has a constant scale height

$$h_d' \approx \tfrac{3}{4}\epsilon^{-1}(L/L_E)R_S, \tag{2.3}$$

where $\epsilon \lesssim 0.1$ is the efficiency of mass-to-energy conversion in the accretion flow, L_E is the Eddington luminosity, and R_S is the Schwarzschild radius. The X-rays must be emitted in a region at least several times R_S in size, whether the central object is a black hole or a neutron star, so the emission region is at least as thick as the inner disk if $L \lesssim 0.3L_E$. Hence the surface of the inner disk is illuminated by the X-rays unless $L \sim L_E$ or unless the X-rays are emitted directly from the surface itself. In Shakura and Sunyaev's models, however, the disk flares once the gas pressure dominates:

$$\frac{h_d}{R_0} = \phi_{dIC}\left(\frac{R_0}{R_{IC}}\right)^s, \tag{2.4}$$

where the constant $\phi_{dIC} = 10^{-3}$ to 10^{-1} and $s = 1/8$ or $1/20$, depending on the source of opacity. Hence, the surface of the gas-pressure dominated disk can always "see" the central source, provided L is not too close to L_E. In what follows we assume that such a direct line of sight exists.

a) *Vertical Structure of the Corona*

Before addressing the problem of radiative transfer in the corona and wind, we first discuss the vertical structure of the corona, including the effects of radiation from the disk itself and thermal conduction.

An isothermal corona above a disk of thickness h_d has an electron density

$$n_e = \frac{p_0}{2kT_{IC}} \exp\left\{-\left[\left(\frac{zR_0}{h_c}\right)^2 + \frac{zR_{IC}h_d}{R_0^2}\right]\right\}, \tag{2.5}$$

where

$$h_c = (2R_0^3/R_{IC})^{1/2} \tag{2.6}$$

is the coronal scale height, zR_0 is the vertical height above the disk, and T_{IC} is defined in equation (I2.4). In the innermost region of the disk, the corona may be thinner than the disk, but for

$$\xi \equiv \frac{R_0}{R_{IC}} > 2\left(\frac{h_d}{R}\right)^2 \equiv \xi_G \tag{2.7}$$

the corona is thicker than the disk and has a Gaussian density profile. We shall assume the thick corona case here.

A lower limit on ξ_G is obtained by using the value of h_d/R for a radiation-pressure dominated disk,

$$\xi_G > 4.7 \times 10^{-3}(L/\epsilon_{-1}L_E)^{2/3}\,, \tag{2.8}$$

where $\epsilon_{-1} = \epsilon/0.1$.

The coronal temperature T_h is governed by Compton heating and cooling by both the radiation from the central source *and* the radiation emitted locally by viscous dissipation in the accretion disk:

$$T_h = \frac{J_d T_d + J T_{IC}}{J_d + J}\,, \tag{2.9}$$

where

$$J_d = \frac{1}{2\pi}\left(\frac{3GM\dot{M}}{8\pi R_0^3}\right) \tag{2.10}$$

is the mean intensity of the radiation emitted by the disk and T_d its inverse Compton temperature ($\approx$effective temperature for a blackbody). Defining

$$f_d \equiv \frac{4\pi J_d}{L/4\pi R^2} = \frac{\xi_{hc}}{\xi} \tag{2.11}$$

with

$$\xi_{hc} = 4.5 \times 10^{-4} T_{IC8}/\epsilon_{-1}\,, \tag{2.12}$$

and neglecting T_d in comparison with T_{IC} (a necessary condition for the corona to be thicker than the disk), we find

$$T_h \approx \frac{f_\Gamma T_{IC}}{f_\Gamma + f_d}\,. \tag{2.13}$$

That part of the corona with $f_\Gamma > f_d$ has $T_h > \frac{1}{2}T_{IC}$, and we term this the "hot corona." With our assumption that $T_d \ll T_{IC}$, the hot corona can exist only if $f_d < 1$, i.e., at radii exceeding $\xi_{hc}R_{IC}$. (For strongly magnetized neutron stars the accretion disk is outside the magnetosphere and is entirely beyond $\xi_{hc}R_{IC}$.) Note that ξ_{hc} exceeds ξ_G, the point at which the corona is thicker than the disk, only for $L \lesssim T_{IC8}^2 \epsilon_1^{-1/2} L_{cr}$, based on the estimate for ξ_G in equation (2.8); L_{cr} is defined in equation (I2.12a).

The transition region between the hot corona and the disk is determined by the variation of f_Γ with height and by thermal conduction. When this transition has a significant thickness, we refer to it as the "cool corona." We do not analyze the structure of this transition region here, but we shall make a few general comments. In a steady state the corona has a negligible mass flux, so the energy equation is

$$-\frac{1}{R_0^2}\frac{d}{dz}\kappa\frac{dT}{dz} = n\Gamma - n^2\Lambda\,, \tag{2.14}$$

where κ is the conductivity, and the pressure p_0 is determined by the condition (Zel'dovich and Pikel'ner 1969)

$$\int_0^\infty (n\Gamma - n^2\Lambda)dz = 0\,. \tag{2.15}$$

If the corona were isobaric and transparent, then this would require $\Xi' \sim \Xi'_{h,\min}$ (which is defined after eq. [I2.1]); however, as we shall see in § II*b*, these conditions are not satisfied in the inner parts of the disk.

Although thermal conduction is important in the interface between the disk and hot corona, we assume that it is not significant in the hot corona itself. Let h_κ be the characteristic thickness of the conductive interface. Since $\kappa \propto T^{5/2}$, the heat flux is

$$\frac{d}{dz}\left(\frac{2}{7}\frac{\kappa T}{R_0}\right) = \frac{2}{7}\frac{\kappa T}{h_\kappa}$$

and since the energy flux to be conducted is $\sim n_e \Gamma f_\Gamma h_\kappa$ we have

$$h_\kappa = \left(\frac{2}{7}\frac{\kappa T}{n_e \Gamma f}\right)^{1/2}\,. \tag{2.16a}$$

Evaluating this at $T = \frac{1}{2}T_{IC}$, where the heating and cooling are no longer in balance, we find

$$\frac{h_\kappa}{h_c} = 6 \times 10^{-4}\frac{L_E}{Lf}(\Xi' T_{IC8}^{3/2}\xi)^{1/2}\,. \tag{2.16b}$$

So long as $h_\kappa \ll h_c$, conduction is confined to a thin boundary layer and may be neglected over most of the hot corona; this is valid provided L/L_E is not too small nor T_{IC} too large. The opposite case of high temperature ($T_h \sim 10^9$ K) with $h_\kappa \sim h_c$ has been considered by Liang and Thompson (1979).

b) Radiative Transfer in the Corona

The uppermost layers of the corona flare and receive unattenuated radiation, so that $T_h \approx T_{IC}$. Deeper in the corona, the radiation from the central source is attenuated by a factor exp $(-\tau_s)$. In general, scattered radiation contributes an amount of f_{sc} to f_Γ, but we defer consideration of this term. The coronal temperature (eq. [2.13]) then becomes

$$T_h = T_{IC}/(1 + f_d e^{\tau_s}) . \tag{2.17}$$

Once τ_s exceeds $\ln f_d^{-1}$, the temperature plummets. Hence the hot corona cannot extend below the point at which $\tau_s = \ln f_d^{-1}$.

In the *inner attenuation zone*, this condition determines the lower boundary of the hot corona, which is at a height h_{hc} above the midplane of the disk:

$$\tau_s(h_{hc}) = \ln f_d^{-1} = \ln (\xi/\xi_{hc}) , \tag{2.18a}$$

or equivalently,

$$f_\Gamma(h_{hc}) = f_d . \tag{2.18b}$$

The value of the characteristic optical depth $\tau_\parallel \equiv n_e \sigma_T R_0$ depends upon the unknown shape of this lower boundary and is uncertain, so we set it equal to a constant k_τ, of order unity. If the line of sight from the central source to an arbitrary point in the hot corona enters the corona at ξ_{min}, then

$$\tau_s(h) = \int_{\xi_{min}}^{\xi} n_e \sigma_T R_{IC} \, d\xi = k_\tau \ln (\xi/\xi_{min}) . \tag{2.19}$$

At the base of the hot corona we have $\tau_s(h_{hc}) = \ln (\xi/\xi_{hc})$, so that

$$\xi_{min}(h_{hc}) = \xi^{1 - 1/k_\tau} \xi_{hc}^{1/k_\tau} . \tag{2.20}$$

To be self-consistent, the base of the hot corona must flare; hence $\xi_{min}(h_{hc})$ must increase with ξ, k_τ must be greater than or equal to 1, and $\xi_{min}(h_{hc})$ must be greater than or equal to ξ_{hc}. In this simple model there are then two cases: (1) the line of sight enters the corona at ξ_{hc} ($\xi_{min} = \xi_{hc}$) and $k_\tau = 1$; or (2) $\xi_{min} > \xi_{hc}$ and $k_\tau > 1$. In the first case $\tau_s(\xi, h)$ is independent of height h; in the second case τ_s is independent of the disk structure only if $\xi_{min} > \xi_G$, whence $h/R_0 = (2\xi_{min})^{1/2}$ and

$$\tau_s(\xi, h) = k_\tau \ln [2\xi(h/R_0)^{-2}] . \tag{2.21}$$

The pressure in the hot corona is related to k_τ by $p = 2kT_{IC} k_\tau/\sigma_T R_0$, so that the ionization parameter at the base of the hot corona is

$$\Xi'(h_{hc}) = \frac{(L/L_E)}{k_\tau \xi} e^{-\tau_s} = \frac{1}{k_\tau}\left(\frac{L}{L_E}\right)\frac{\xi_{hc}}{\xi^2} = \frac{4.5 \times 10^{-4}}{k_\tau}\left(\frac{L}{L_E}\right)\frac{T_{IC8}}{\epsilon_{-1}\xi^2} . \tag{2.22}$$

Thus, as one moves outward in the inner attenuation zone, $f_d = \xi_{hc}/\xi$ drops, the optical depth rises, and $\Xi'(h_{hc})$ drops. When $\Xi'(h_{hc})$ reaches its minimum possible value, $\Xi'_{h,min}$, the inner attenuation zone terminates; we label this point ξ_{ia}:

$$\xi_{ia} = \left[\frac{\xi_{hc}(L/L_E)}{k_\tau \Xi'_{h,min}}\right]^{1/2} = 0.021\left[\frac{T_{IC8}(L/L_E)}{k_\tau \Xi'_{h,min}\epsilon_{-1}}\right]^{1/2} . \tag{2.23}$$

Note that for a star, $R_{ia} = \xi_{ia} R_{IC} \sim 2 \times 10^8 (L/L_E)^{1/2}(M/M_\odot)$ cm, which is comparable to the radius of the magnetosphere of a strongly magnetized neutron star and to the radius of a white dwarf; in either case the inner attenuation zone would be severely truncated.

Outside the inner attenuation zone the ionization parameter is approximately constant so that $\tau_\parallel$ drops as ξ increases. Since the optical depth in this zone is determined by attenuation in interior parts of the corona, we term this the *shadowed zone*. In the *inner* shadowed zone, the attenuation at the base of the hot corona is unchanged from that at the boundary of the inner attenuation zone

$$f_{is} = f_\Gamma(\xi_{ia}, h_{hc}) = \frac{\xi_{hc}}{\xi_{ia}} = 0.021\left[\frac{T_{IC8} k_\tau \Xi'_{h,min}}{\epsilon_{-1}(L/L_E)}\right]^{1/2} \tag{2.24}$$

so that

$$\tau_\parallel \equiv n_e \sigma_T R_0 = k_\tau(\xi_{ia}/\xi) . \tag{2.25}$$

If the disk flares sufficiently, then it will force the base of the hot corona into a region where the attenuation factor f is closer to unity. Since f is still determined by scattering in the inner attenuation zone, we term this the *outer* shadowed zone. Two conditions must be satisfied in this zone: the disk must be out of the shadow of the cool corona in the inner attenuation zone ($h_d/R > h_{hc}/R$); and the line of sight from the disk to the central source must exit the corona at $\xi_{min} > \xi_{hc}$ so that $f > f_{is}$. The transition between the hot corona and the surface of the disk is thin in this zone—there is no "cool corona." Denote the boundary between the two shadowed zones by ξ_{is}. For a thick corona ($\xi_{min} > \xi_G$, or $L \lesssim T_{IC8}^2 \epsilon_{-1}^{-1/2} L_{cr}$) equation (2.21) can be used to show

$$\phi_{dIC}\, \xi_{is}^{s} = (2\xi_{hc})^{1/2} (\xi_{ia}/\xi_{hc})^{0.5(1-1/k_\tau)} ; \tag{2.26}$$

and in the outer shadowed zone the attenuation factor is

$$f = f_{is} (\xi/\xi_{is})^{2sk_\tau} . \tag{2.27}$$

On the other hand, for a thin corona ($\xi_{min} < \xi_G$) both ξ_{is} and f depend on the uncertain shape of the disk at small radii.

At sufficiently large radii $f \to 1$ and we enter the *outer attenuation zone*, in which f is once again determined by local scattering rather than by attenuation in the inner corona. This zone begins only where the line of sight from the disk photosphere to the central source clears the corona at ξ_{ia} [i.e., $h_d/R > (2\xi_{ia})^{1/2}$]. The outer boundary of the outer shadowed zone at ξ_{os} is generally in the wind region of the disk ($\xi_{os} > 1$) and is discussed below.

The approximate classification of different zones in the disk is predicated on the assumption that $\Xi_0' > \Xi_{h,min}'$ in the inner attenuation zone, or equivalently, that the outer boundary of the inner attenuation zone at ξ_{ia} be beyond the inner boundary at ξ_{hc}. This is true if

$$L > k_\tau\, \xi_{hc}\, \Xi_{h,min}'\, L_E = 4.5 \times 10^{-4} k_\tau\, T_{IC8}\, \epsilon_{-1}^{-1} \Xi_{h,min}'\, L_E , \tag{2.28}$$

corresponding roughly to $L \gtrsim 10^{-2} L_{cr}$. Below this luminosity, the corona is completely transparent and $f = 1$. For example, cataclysmic variables have small enough X-ray luminosities (Córdova, Mason, and Nelson 1981) to fall into this regime. Thermal conduction is likely to be important in such coronae (eq. [2.16b]).

Heretofore we have neglected the effect of radiation from the central source which has been scattered by the corona. This scattered radiation is unimportant to the structure of the hot corona, but it is important to the cool corona. Below we show that the electron scattering optical depth $\tau_\perp$ normal to the disk is always small (eqs. [2.35] and [3.10]), which greatly simplifies the analysis since multiple scattering can be neglected. In the inner attenuation zone, the contribution to f_Γ due to single scattering is

$$f_{sc} \approx \frac{1}{2} \frac{S_\perp \ln \tau_\perp^{-1}}{L/4\pi R_0^2} = \frac{k_\tau}{2k_\tau + 1} \left(\frac{\xi}{2}\right)^{1/2} \ln \tau_\perp^{-1} , \tag{2.29}$$

where $S_\perp$ is the scattered surface brightness normal to the disk (eqs. [3.5]–[3.11]). In the shadowed zone, the local contribution to scattering declines steadily, so that $f_{sc} < f_{sc}(\xi_{ia})$. The condition that scattering be negligible in the hot corona is $f_{sc}/f_\Gamma(h_{hc}) < 1$; evaluating this ratio at ξ_{ia}, where it is a maximum, gives

$$\frac{L}{L_E} < 0.5 \Xi_{h,min}' \left(\frac{T_{IC8}}{\epsilon_{-1}}\right)^{1/3} \left(\frac{1}{\ln \tau_\perp^{-1}}\right)^{4/3} \tag{2.30}$$

for $k_\tau \sim 1$. Except for luminosities very near the Eddington limit, scattered radiation is indeed negligible compared with direct attenuated radiation in the hot corona. At these high luminosities, one can show that a corona could be maintained solely by scattering out to a radius

$$\xi_{sc} \sim \left(\frac{L}{\Xi_0' L_E}\right)^2 . \tag{2.31}$$

For $L/L_E \lesssim \frac{1}{3}$, this implies $\xi_{sc} \lesssim 0.1$; since a wind arises only for $\xi \gtrsim 0.1$ (Paper I), we conclude that it is impossible for a wind to be maintained solely by scattering under these conditions. In other words, self-excited winds cannot exist except perhaps at large luminosities.

Scattered radiation is quite important in determining what goes on below the hot corona in the inner attenuation zone. Recall that at the base of the hot corona, the radiation from the central source has been attenuated sufficiently that the coronal temperature is beginning to drop below T_{IC}. Below that hot corona, the equilibrium Compton temperature is

$$T_{eq} = \frac{J_d T_d + J_{sc} T_{IC}}{J_d + J_{sc}} = \frac{f_d T_d + f_{sc} T_{IC}}{f_d + f_{sc}} , \tag{2.32}$$

where J_{sc} is the mean intensity of the scattered radiation. For $T_{eq} \lesssim 10^7$ K, this will only be a rough approximation

to the gas temperature, since line cooling and photoionization heating may become important. Scattered radiation will create a "cool corona" if $T_{IC} \gg T_{eq} \gg T_d$, and one can show that this occurs in the inner attenuation zone for

$$\xi \gtrsim 1.6 \times 10^{-3} \left[\left(\frac{L}{L_E} \right) \left(\frac{M_\odot}{M} \right) \frac{T_{IC8}^3}{\epsilon_{-1}^5} \right]^{1/9} . \tag{2.33}$$

For binary X-ray sources this is most of the inner attenuation zone, and for quasars it comprises the entire zone.

c) *Radiative Transfer in the Wind*

In Paper I we divided the wind and corona into five regions (A–E) based on the luminosity of the central source and the radius (see Fig. I.1): Region A is an isothermal wind unaffected by gravity ($L/L_{cr} > \xi > 1$); Region B is steadily heated wind also unaffected by gravity [$\xi > \max (L/L_{cr}, L_{cr}^2/L^2) > 1$]; Region C is a steadily heated, gravitationally inhibited wind ($L_{cr}^2/L^2 > \xi > 1$); Region D is a corona with a non-isothermal wind ($\xi < 1$, $L/L_{cr} < 1$); and Region E is a corona with an isothermal wind ($\xi < 1$, $L/L_{cr} > 1$). First we demonstrate that this classification is insensitive to radiative transfer effects. The dividing radius between wind and corona remains R_{IC} since the temperature in the upper corona is always close to T_{IC} (except at very small radii, $\xi < \xi_{hc}$). The condition that the wind be in Region A is that T reach T_{IC} for $z \lesssim O(1)$. Likewise, the classification in Regions B and C depends on the heating rate at $z \sim O(1)$, where the flows reach their maximum temperatures. Hence, the relevant optical depth for the classification is $\tau_s(z \sim 1)$, the line-of-sight optical depth from $z \sim 1$ to the source. Such lines of sight remain at $z \approx 1$ for all R, and miss the optically thick part of the corona entirely. Since the horizontal and vertical optical depths are comparable, we evaluate the latter. In Region A we set $T \approx T_{IC}$ and $2n_e k T_{IC} = \frac{1}{2} p_0$. In Regions B and C we slightly overestimate n_e by computing p/T from equations (I2.11), (I3.13), (I3.19), and (I3.21), and by setting the factor $(p^*/\eta)^{1/2} (f_\Gamma / y^{\langle \beta \rangle})^{-1/4} \approx 1$. The results are

$$\tau_\perp \equiv \int_1^2 n_e \sigma_T R_0 \, dy = \frac{Lf}{L_E \Xi_0'} \begin{cases} 0.5 \xi^{-1} & \text{(Region A)} \\ \dfrac{3.6}{\xi^{1/3}} \left(\dfrac{L_{cr}}{L} \right)^{2/3} & \text{(Region B)} \\ 9 & \text{(Region C)} . \end{cases} \tag{2.34}$$

Taking into account the boundaries of the various regions, we find

$$\tau_\perp < (f/\Xi_0') [0.5, 0.1 T_{IC8}^{-1/2}, 0.3 T_{IC8}^{-1/2}] \tag{2.35}$$

in Regions A, B, and C, respectively. Since $\Xi_0' \sim \Xi_{c,\max}' \gtrsim \frac{1}{2}$ and $T_{IC8} > 0.1$ for systems of interest, and since $f < 1$ always, we conclude that $\tau_\perp$, and hence $\tau_s(z \sim 1)$, are less than unity for all wind solutions. Thus, our classification scheme is preserved; and in treating the radiative transfer, multiple scattering can be neglected.

The base of the wind will lie in the shadow of the inner attenuation zone unless the disk is relatively thick, $(h_d/R) \gtrsim 0.2$ according to the rough estimate below equation (2.27), or unless L is so low that the corona is transparent (eq. [2.28]). Attenuation in the wind itself may be important even though $\tau_s(z \sim 1) \sim \tau_\perp \ll 1$ because lines of sight from the base of the flow to the central source pass through dense regions at $z \ll 1$. However, the analysis in Appendix B shows that f_{wind} usually exceeds 0.1 (see eqs. [B10] and [B11]).

III. SCATTERED RADIATION

a) *Scattered X-Ray Surface Brightness and Luminosity*

A Compton-heated corona or wind is an extended source of scattered X-rays. Since the optical depth $\tau_\perp$ normal to the disk is small (cf. § II*b*, *c*), only single scattering is important and the local scattering emissivity at a distance R from the central source is

$$j_{sc} = \frac{n_e \sigma_T L}{(4\pi)^2 R^2} e^{-\tau_s} . \tag{3.1}$$

For observational purposes, the most detailed diagnostic of scattering is the integral of j_{sc} along a line of sight through the source, the surface brightness

$$S = \int j_{sc} e^{-\tau_{ob}} dl . \tag{3.2}$$

Here τ_{ob} is the optical depth along the line of sight to the scattering point. The quantity τ_{ob} may be appreciable for lines of sight which pass through the corona at $R/R_{IC} \lesssim \xi_{ia}$ or through the wind at $h/R \ll 1$.

i) *Scattering in the Wind*

In this section we draw heavily on the results of §§ II and III, Paper I. The surface brightness S for a disk at an arbitrary angle i to the line of sight is a rather complicated function, so we focus on the two extreme cases of a face-on disk ($S_\perp$) and an edge-on disk ($S_\parallel$). Far from the disk the wind has a constant velocity and $n_e \propto R^{-2}$; closer to the disk, n_e must be consistent with the value of $\tau_\perp$ calculated in equation (2.34). Hence n_e must be of the form

$$n_e \approx \left.\frac{R_0\,\tau_\perp(R_0)}{\sigma_T R^2}\right|_{R_0=\min(R,R_d)}, \tag{3.3}$$

where the condition on R_0 accounts for the fact that for $R < R_d$, gas originating at $R_0 \sim R$ determines n_e, whereas for $R > R_d$ the gas originates at $R_0 \sim R_d$; here R_d is the outer radius of the disk. This approximation averages over the $(y-1)^{-1/2}$ variation of n_e with height above the plane found in § III, Paper I, for Regions B and C, and so it is suitable for calculating $S_\perp$ but not $S_\parallel$. Evaluation of $S_\perp$ from equation (3.2) with the aid of equations (3.1) and (3.3) yields

$$S_\perp \approx \frac{LR_0\,\tau_\perp(R_0)}{(4\pi)^2 R_t^3} \tag{3.4}$$

$$= \left[\frac{L}{(4\pi)^2 R_{IC}^2}\right]\frac{Lf(\xi_t)}{L_E\,\Xi_0'}\begin{cases}\dfrac{1}{2\xi_t^3} & \text{(A)}\\[2ex] 3.6\left(\dfrac{L_{cr}}{L}\right)^{2/3}\dfrac{\xi^{2/3}}{\xi_t^3} & \text{(B)}\\[2ex] 9\,\dfrac{\xi}{\xi_t^3} & \text{(C)}\end{cases}. \tag{3.5}$$

Here $\xi_t \equiv R_t/R_{IC}$ is the normalized distance of closest approach of the line of sight to the central source; as in equation (3.3), $\xi \equiv R_0/R_{IC} = \min(\xi_t, \xi_d)$. We have ignored τ_s in equation (3.1) since it is significant only for $h \ll R$, which does not contribute much to $S_\perp$; since $\tau_{ob} = \tau_\perp \ll 1$, we have ignored τ_{ob} as well.

If the disk is edge-on, S is not very different from $S_\perp$ in Region A or, if $R \gg R_d$, in Regions B and C, since in both cases the flow is roughly spherical. However, if $R \leq R_d$ in Region B or C, the density becomes large near the surface of the disk, and equation (3.3) for n_e must be replaced by (see eqs. [I3.32] and [I3.41] for $T^* \propto n^{-1}$)

$$n_e \approx \frac{1}{2}\frac{\tau_\perp(R_0)}{\sigma_T R_0 z^{1/2}}. \tag{3.6}$$

For simplicity, any variation in the heating rate (f_Γ) along a streamline has been ignored. Optical depth effects become important for $\tau_\parallel = n_e \sigma_T R_0 > 1$, or $z^{1/2} \sim (h/R_0)^{1/2} < \tau_\perp/2$. Integration of equation (3.2) then gives

$$S_\parallel \approx \frac{S_\perp}{(h/R_t)^{1/2} + (1/2)\tau_\perp(R_0)} \quad \text{(B, C)}, \tag{3.7}$$

where the $\tau_\perp/2$ term causes $S_\parallel$ to saturate when $\tau_\parallel > 1$. Note that for an edge-on disk $R_t^2 \gtrsim h^2 + R_0^2$, so $h/R_t < 1$.

The total scattered luminosity due to the wind

$$L_{sc} = \int_{R_{IC}}^{\infty} 4\pi j_{sc}\,dV \tag{3.8}$$

is dominated by the region $R_t < R_d$ and is of order $L\tau_\perp(\xi = 1)$; more precisely,

$$\frac{L_{sc}}{L} = \frac{Lf}{L_E\,\Xi_0'}\begin{cases}\frac{1}{2} & \text{(A)}\\[2ex] \left(\dfrac{L_{cr}}{L}\right)^{2/3}(11 - 7\xi_d^{-1/3}) & \text{(B)}\\[2ex] 9(1 + \ln\xi_d) & \text{(C)}\end{cases}. \tag{3.9}$$

This is generally small since f is reduced by shadowing when $L \to L_E$. Somewhat less than half of the scattered X-rays will be absorbed by the disk, so the scattered luminosity actually escaping the system will be somewhat greater than half the value in equation (3.9).

ii) *Scattering in the Corona*

In the corona, the surface brightness depends on whether the line of sight passes through the inner attenuation zone ($\xi_{hc} < \xi < \xi_{ia}$) or the shadowed zone ($\xi_{ia} < \xi < \xi_{os}$). We focus on the case ($\xi_t \ll 1$, $\xi_t < \xi_d$), so that the effects

of the coronal wind are negligible and S can be calculated in the same manner for both Regions D and E. Recall that in the inner attenuation zone $n_e \sigma_T R_0 = k_\tau$ (eq. [2.19]). In the inner shadowed zone $n_e \sigma_T R_0 = k_\tau(\xi_{ia}/\xi)$ (eq. [2.25]); in the outer shadowed zone, n_e is increased by a factor f/f_{is} (eq. [2.27]), but since this factor is not large, we ignore it. Since the height of the corona is $h_c = (2\xi)^{1/2} R_0$, we find that over the entire corona

$$\tau_\perp \approx \frac{k_\tau (2\xi)^{1/2}}{1 + \xi/\xi_{ia}} . \tag{3.10}$$

Since ξ_{ia} is small (eq. [2.23]), $\tau_\perp$ is also. In the inner attenuation zone, τ_s is given by equation (2.21) over most of the volume of the corona, whereas for $\xi \gg \xi_{ia}$, τ_s is negligible. The perpendicular (face-on) surface brightness in the inner attenuation and inner shadowed zones can be approximated by a single expression

$$S_\perp \approx \frac{L}{(4\pi)^2 R_{IC}^2} \frac{2^{1/2} k_\tau}{\xi_t^{3/2}(1 + 2k_\tau + \xi_t/\xi_{ia})} . \tag{3.11}$$

If the outer part of the corona is in the outer shadowed zone ($\xi_{is} < 1$: eq. 2.26), then $S_\perp$ is larger there by a factor f/f_{is} [eq. (2.27)].

In the inner attenuation zone, the scattered luminosity inside ξ is

$$L_{sc}(<\xi) = \int_0^\xi 2\pi R_{IC}^2 \, \xi d\xi \int_0^{h_c} 4\pi j_{sc} \, dh \tag{3.12}$$

$$= \frac{k_\tau (2\xi)^{1/2}}{(2k_\tau + 1)} L . \tag{3.13}$$

We have assumed that half the scattered radiation is absorbed by the disk, which is somewhat of an overestimate for $h\nu > 10$ keV. For $k_\tau \gg 1$, equation (3.13) is just what one would expect: in the optically thick limit, half the radiation with $(h/R) < h_c/R = (2\xi)^{1/2}$ is scattered away from the disk; as seen from the central source, this is just the fraction of the sky covered by that part of the corona inside ξ (counting both sides of the disk), whence $L_{sc}/L = \frac{1}{2}(2\xi)^{1/2}$.

In the shadowed zone, $S \propto \xi^{-5/2}$ and L_{sc} converges. Using the approximation (3.11), we find the total luminosity scattered by the corona, including both the inner attenuation and inner shadowed zones, is

$$\frac{L_{sc}}{L} \approx \frac{2^{-1/2} \pi k_\tau}{1 + 2k_\tau} [(1 + 2k_\tau)\xi_{ia}]^{1/2} \tag{3.14}$$

$$\approx 0.19 \left[\frac{T_{IC8}(L/L_E)}{\Xi'_{h,\min} \epsilon_{-1}} \right]^{1/4} , \tag{3.15}$$

where we set $k_\tau = 1$ in the last equation for simplicity. [Scattering by the outer shadowed zone depends on the geometry of the disk and has not been calculated. It is important only if the disk flares sufficiently that $f \sim O(1)$, and then it could be comparable to the scattering by the wind.] In view of the weak dependence on the parameters, we conclude that the corona will scatter a significant fraction of the luminosity from the central source under a wide range of conditions.

The effects of scattering are most apparent in sources observed edge-on ($i \approx 90°$). The central source may be obscured by the disk, leaving only the scattered X-rays visible. The surface brightness depends on the optical depth

$$\begin{aligned} \tau_{ob} &= k_\tau(1 + \ln \xi_{ia}/\xi) \quad (\xi < \xi_{ia}) \\ &= k_\tau \xi_{ia}/\xi \qquad\quad (\xi > \xi_{ia}) \end{aligned} \tag{3.16}$$

from ξ out to the observer. Let ξ_1 be the value of ξ at which $\tau_{ob} = 1$,

$$\xi_1 \approx \xi_{ia}/[\exp(1/k_\tau) - 1] . \tag{3.17}$$

For $\xi_t > \xi_1$, the corona is optically thin and $S_\parallel$ is (R_t/h) times larger than $S_\perp$. For $\xi_t < \xi_1$, the corona is optically thick along the line of sight, and the observed emission is dominated by gas at ξ_1. Hence the edge-on surface brightness of a disk is

$$S_\parallel(\xi_t) \approx (2\xi)^{-1/2} S_\perp(\xi) \Big|_{\xi = \max(\xi_t, \xi_1)} , \tag{3.18}$$

where $S_\perp(\xi)$ is given in equation (3.11).

If the disk is eclipsed, the light curve is determined by the integral of $S_\parallel$ over height above the disk. Let

$L_{sc}^{obs}(<\xi_t)$ be the observed luminosity (i.e., $4\pi \times$ distance$^2 \times$ observed flux) of the scattered X-rays inside ξ_t. Counting the top and bottom, and right and left sides of the disk, we have

$$\frac{dL_{sc}^{obs}}{d\xi_t} = 4\pi S_{\parallel} \cdot 4h \tag{3.19a}$$

$$= \frac{2^{1/2} L k_\tau}{\pi \xi^{1/2}(1 + 2k_\tau + \xi/\xi_{ia})}\bigg|_{\xi = \max(\xi_t, \xi_1)} \tag{3.19b}$$

for an edge-on disk. (If ξ_t is in the outer shadowed zone, this should be increased by f/f_{is}.) Integrated over the entire disk, L_{sc}^{obs} is about $(2/\pi)$ times the total scattered luminosity L_{sc} in equation (3.15):

$$\frac{L_{sc}^{obs}(\text{edge-on})}{L} \approx 0.1 \left[\frac{T_{IC8}(L/L_E)}{\Xi'_{h,\min}\epsilon_{-1}}\right]^{1/4}. \tag{3.20}$$

For a binary X-ray source, the typical radius at which the scattering occurs is $R_{ia} \sim 2 \times 10^8 (L/L_E)^{1/2}$ cm, so entrance and exit from X-ray eclipses should last a time of order $2R_{ia}/v_{orbital}$; scattering in the atmosphere of the companion star could lengthen this. The scattered X-rays should be highly polarized (§ III*c*). If i is close enough to 90° that $\cos i < h_d(\xi_d)/R_d$, then even these scattered X-rays will be obscured by the disk, and only X-rays scattered from the outer disk and the wind will be visible.

iii) *Comparison of Scattering in Wind and Corona*

The scattered luminosity from the corona (eq. [3.15]) is insensitive to the source parameters and occurs primarily at small radii $\sim R_{ia}$. The scattered luminosity from the wind (eq. [3.9]) varies linearly with L in Regions A and C and also varies directly as the uncertain attenuation factor f. Taking the ratio of the two equations, we find

$$\frac{L_{sc}(\text{wind})}{L_{sc}(\text{corona})} \approx \left(\frac{L}{L_{cr}}\right)^{3/4} \frac{\epsilon_{-1}^{1/4} f}{\Xi_0'^{3/4} T_{IC8}^{5/8}} \begin{cases} 0.2 & \text{(A)} \\ 2\left(\frac{L_{cr}}{L}\right)^{2/3} & \text{(B)} \\ 4 & \text{(C)}, \end{cases} \tag{3.21}$$

where we have set $\xi_d = O(1)$. In Region A, $L_{sc}(\text{wind})/L_{sc}(\text{corona})$ can reach $2.5(L/L_E)^{3/4} f$ for $\epsilon_{-1} \sim T_{IC8} \sim \Xi'_{h,\min} \sim 1$, but f is likely to be small for $L \sim L_E$. Note that in Region B, we have $L_{sc}(\text{wind}) \sim f L_{sc}(\text{corona})$ for a wide range of L. If $f \sim 1$, as it may be in Regions B and C for a thick, flaring disk, then the scattered luminosity is concentrated at two different radii: $R \sim R_{ia} \ll R_{IC}$ in the corona and $R \sim R_{IC}$ to R_d in the wind. The intermediate region is in the shadowed zone and contributes relatively little to the scattered radiation.

b) Eclipses of Corona and Wind in X-Ray Binaries

The most direct observational evidence for scattering by a Compton-heated corona or wind comes from the X-ray binaries 4U 2129+47 and 4U 1822−37 (cf. White *et al.* 1981; White and Holt 1982; McClintock *et al.* 1982; and references therein), which exhibit partial eclipses of their X-ray sources. The constancy of the X-ray spectrum during eclipses, coupled with the eclipses' partiality, have led the above-mentioned authors to suggest that the observed X-rays have been scattered by an extended corona or wind. Other sources show similar evidence for scattering from an extended corona, during non-eclipse modulation of the X-ray brightness. For example, both Her X-1 and Cen X-3 show persistent emission during their extended "low" phases, without the soft X-ray cutoff that would be expected if the entire source were obscured by photoelectric absorption (Holt and McCray 1982). However, in this discussion we will focus on the two partially eclipsing binaries.

The eclipse light curves carry information about the surface brightness distribution of the X-ray sources, as well as the sizes and apparent trajectories of the occulting bodies. The smoothness of the light curves in both sources indicates that there is no central region of the X-ray source that is much brighter than the rest. In particular, direct X-rays from the region surrounding the compact accreting body are completely obscured, either by the flaring disk or by optically thick regions of the corona/wind at $z \ll 1$. By assuming ad hoc that the X-ray source is a disk or sphere of uniform surface brightness, White and Holt (1982) and McClintock *et al.* (1982) have fitted the light curves of 4U 1822−37 and 4U 2129+47, respectively. To reproduce the pointy minima, the occulting star must be nearly tangent to the sharp edge of the X-ray source at mid-eclipse, and hence the star and source must be of comparable size. The steadily sloping sides of the light curves require that the vertically integrated brightness distribution ($dL_{sc}^{obs}/d\xi_t$; cf. § III*a*) of the source not be very centrally peaked.

We have compared the observed light curves with the family of light curves that would be produced if the scattered brightness had the distributions associated with our physical models for the corona and wind given in § III*a*. We shall go into some detail since such a comparison can provide a stringent test of the models. McClintock *et al.* (1982) developed a model for the corona which gives a surface brightness distribution which is similar to that

found in § III*a*, although they did not use this model in their comparison with observation. Our results represent an improvement on theirs in that we drop the assumption of uniform surface brightness in comparing with observation, we include scattering from the wind, and we demonstrate that the inferred disk size is consistent with that expected from truncation by a Compton-heated wind (Paper I). We find that lines of sight which pass through the corona at $\xi_t < \xi_{ia}$ do indeed pick up a rather flat distribution of $dL_{sc}^{obs}/d\xi_t$ (eq. [3.19b]), but for parameters characterizing X-ray binaries this region is too small to dominate the behavior of the light curve. In fact, in order for $dL_{sc}^{obs}/d\xi_t$ to be flat, the corona in both the inner attenuation and inner shadowed zones must be obscured by the flaring disk. For an edge-on disk, this requirement is

$$h_d(R_d) > 2^{1/2}\xi_{is}^{3/2}R_{IC}\,, \tag{3.22}$$

where ξ_{is} is determined by equation (2.26). Furthermore, we infer that the disk is no more than $\sim[h_d/(R_d + R_{is})]$ radians away from being edge-on. For a disk with $h_d(R_d)/R_d \sim 0.1$, this implies $i \gtrsim 84°$. It seems hard to produce a sufficiently flat brightness distribution if the disk extends much beyond R_{IC}, owing both to the steepness of $dL_{sc}^{obs}/d\xi_t$ in the wind zone and to the difficulty of obscuring a wind geometrically.

Interpreting the sharp eclipse minima in terms of our physical model is trickier. The scattered X-ray source produced by a wind does not have a sharp "edge," but rather has surface brightness falling off as ξ_t^{-3} for ξ_t well outside the disk radius ξ_d. If such a brightness distribution joined continuously on to a much flatter distribution of $dL_{sc}^{obs}/d\xi_t$ in the region where the occulting star moves across the source, then the resulting light curve would have too broad a minimum. One way around this problem is to suppose that the disk truncates at a radius $\xi_d < 0.1$, in which case the scattering off the wind would be exponentially smaller than that associated with the corona. The source would appear to cut off sharply on a scale $\sim\xi_d$, and would in fact resemble the ad hoc sources considered by White and Holt (1982) and McClintock *et al.* (1982). However, to make the eclipse duration consistent with such a small X-ray source, we would be forced to assume either that the compact object is much more massive than the canonical neutron star mass of 1.4 $M_\odot$, or that the inverse Compton temperature T_{IC} is smaller $\sim 4 \times 10^6$ K, a factor $\gtrsim 6$ lower than the 2.3×10^7 K indicated by the *HEAO 1* observations of White and Holt (1982) (if their data are fitted by a partially Comptonized bremsstrahlung spectrum with a cutoff at 8 keV).

A second, more likely way to account for the sharpness of the eclipses minima is to consider the two-dimensional distribution of surface brightness in the wind at $\xi \gtrsim \xi_d$ (Fig. 2*a*). Over some solid angle fanning out above and below the disk, the run of brightness varies smoothly from $S \propto z^{-3}$ at large z (eq. [3.5]) to some flatter distribution at $z < 1$. For an optically thick steadily heated zone, S can continue to increase as rapidly as $z^{-1/2}$ all the way down to the disk surface (eq. [3.7]). However, off to the side of the disk, the mass flux in the wind and the associated scattered surface brightness must be considerably smaller because streamlines coming off the disk at $\xi \lesssim \xi_d$ are forced outward to fill the void where there is no disk to provide a counterpressure. As a result, the divergence of these streamlines is greater, the critical (sonic) surface is closer to the surface, and the density of wind material filling the solid angle surrounding the equatorial plane at $\xi > \xi_d$ is several times smaller than that filling the solid angle above and below the disk at a comparable distance. In principle, this dropoff in scattered brightness in the region traversed by the occulting star can explain the sharpness of the eclipse minima. Unfortunately, our one-dimensional theory does not allow us to predict the two-dimensional distribution of surface brightness quantitatively. We have, nevertheless, computed eclipse profiles for the class of brightness distributions depicted in Figure 2*a*, which incorporates the main features described above. Varying the angle of the wind θ_0 between 24° and 60° has remarkably little effect on the fit to the light curve of 4U 2129+47 (Fig. 2*b*), although the best overall fit corresponds to $\theta_0 \sim 40°$–$45°$. The ratio of the occulting star's radius (R_{opt}) to that of the disk was chosen to obtain the correct intensity at mid-eclipse. For 4U 2129+47, with 30% of the flux visible at minimum, R_{opt}/R_d varied between 1.00 at $\theta_0 = 24.^\circ13$ and 2.16 at $\theta_0 = 60°$, with a range of 1.2–1.4 for the best overall fits. While only two-dimensional numerical simulations will yield a quantitative description of the distribution of scattered X-ray intensity, we are encouraged that a class of models chosen on the basis of the physical arguments above is able to fit the data reasonably well.

We can use measurements of the eclipse duration to estimate the size of the disk in 4U 2129+47 (duration = 0.1 × period). In units of the binary separation, a, we have

$$R_d + R_{opt} = 0.1(2\pi a)\,, \tag{3.23}$$

which gives R_d/a in the range 0.2–0.3 for the extreme range of R_{opt}/R_d considered above (1–2.16). Let us compare this estimate with the values of R_d predicted by various models for disk truncation. First we show that it is unlikely that the disk is as small as the effective injection radius R_{in} (Flannery 1975), which is given by equation (I4.19). For a star of mass $0.3\ M_\odot \le M_{opt} \le 1\ M_\odot$ and compact X-ray source with $M_x \approx 1.4\ M_\odot$, the mass ratio $\tilde{\mu} \equiv M_x/(M_x + M_{opt})$ lies between 0.58 and 0.82, corresponding to $R_{in}/a = 0.10$ and 0.16, respectively. Combining this with the range of R_d/a inferred above gives $1.3 < R_d/R_{in} < 3$. The disk could be as small as R_{in} only if $\tilde{\mu}$ were large (>0.9) and if R_d/a were at the lower limit of 0.2. Next, the Paczyński-Smak radius R_{max} (eq. [I4.20] and Fig. I.4) intersects the estimated range of R_d at mass ratios $\tilde{\mu}$ between 0.25 and 0.5, too small for a binary

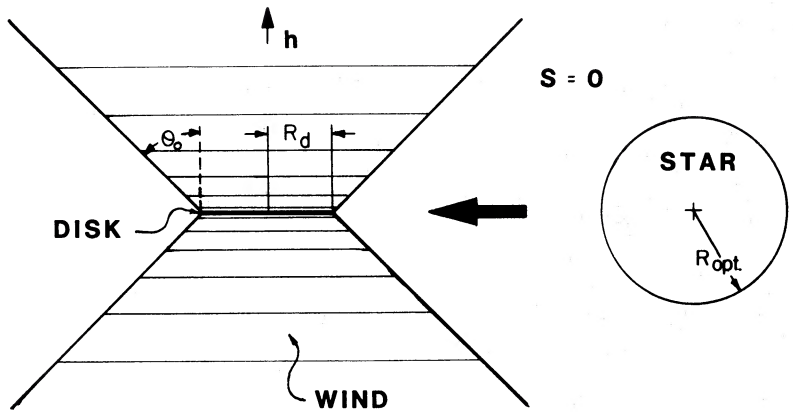

FIG. 2*a*

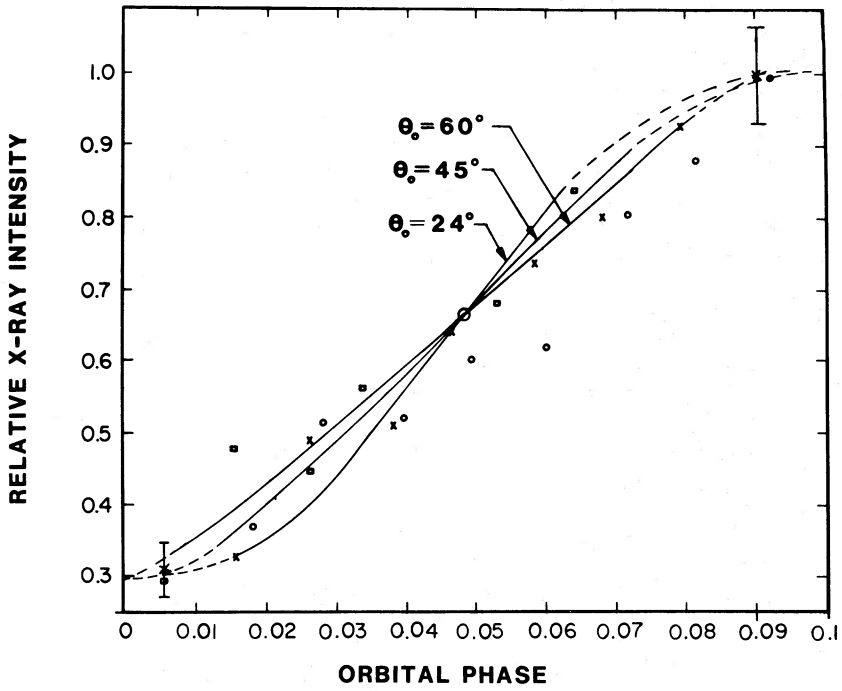

FIG. 2*b*

FIG. 2*a*.—Physically motivated distribution of scattered X-ray surface brightness (S) used to compute the eclipse light curves shown in Fig. 2*b*. The star (radius R_{opt}) moves across the source horizontally, and the ratio R_{opt}/R_d is chosen to normalize the depth of the eclipse to the observed value, 30% in the case of 4U 2129+47. The horizontal lines across the source suggest the contours of constant S, which is taken to vary with h according to $S \propto h^{-1/2}(R_d + h)^{-5/2}$. This scaling simulates the scattering from a wind both near the disk surface ($z \ll 1$) and at $z \gtrsim 1$ (cf. § III*a*; eqs. [3.7] and [3.18]).

FIG. 2*b*.—Eclipse light curves computed for 4U 2129+47 using the brightness distribution illustrated in Fig. 2*a*, plotted against data from McClintock *et al.* (1982). Dashed portions are analytic extrapolations to computed curves. The orbital phase scaling has been selected to give a relative X-ray brightness of 0.65 at phase 0.0474. Data have been folded about mid-eclipse (*circles*, postminimum; *squares and crosses*, preminimum), and typical error bars are shown at upper right and lower left. Computations shown assumed an edge-on inclination for the binary's orbital plane ($i = 90°$), but deviations from this have a less dramatic effect on the estimated values of R_{opt}/R_d here than they do in the case of McClintock *et al.*'s models, because the surface brightness trails off gradually above and below the orbital plane.

containing a 1.4 $M_\odot$ neutron star and a main sequence dwarf. However, disk truncation through angular momentum loss in a wind does appear consistent with the data. Normalizing T_{IC} relative to the 2.3×10^7 K value inferred from White and Holt (1982), we find

$$\xi_{in} = 1.9\left(\frac{R_{in}}{a}\right)\left(\frac{T_{IC}}{2.3 \times 10^7\ \mathrm{K}}\right)\left(\frac{P}{5.2\ \mathrm{hr}}\right)^{2/3}\left(\frac{1.4\ M_\odot}{M_x}\right)^{2/3}\tilde{\mu}^{-1/3}, \tag{3.24}$$

where P is the orbital period. Within the range of mass ratios considered above ($0.58 \leq \tilde{\mu} \leq 0.82$), this gives $0.23 < \xi_{in} < 0.32$. Reference to Figure I.4 shows that for $L/L_{cr} \sim 1$, this value of ξ_{in} together with the requirement $R_d/R_{in} < 3$ implies $\dot{M}_{ch}/\dot{M}_a > 5$, whereas for $L/L_{cr} \sim 10$ it implies $\dot{M}_{ch}/\dot{M}_a > 3$; here $\dot{M}_{ch}$ is the characteristic mass loss rate in the wind (eq. [I4.2]) and $\dot{M}_a$ is the accretion rate by the central object. Since $\xi_d = R_d/R_{IC} = (R_d/R_{in})\xi_{in}$ lies between 0.3 and 1, the total wind mass loss $\dot{M}_w$ is of order $\dot{M}_{ch}$ and hence exceeds the accretion rate $\dot{M}_a$. The discussion of equation (I4.10) suggests that the accretion should be unstable in this case, which would result in fluctuations in the luminosity. Equation (I4.13) gives an uncertain estimate of ~ 10 hr for the characteristic time scale of the instability (with $\alpha_d \sim 1$, $M \sim 1.4\ M_\odot$, $h_d' \sim R/20$, and $T_{IC8} \sim 0.25$). We have no estimate of the expected amplitude of the fluctuations, but an observational search would be worthwhile. This estimate of the mass loss sets a lower limit on the attenuation factor, $f \gtrsim 0.1$ for $L \sim L_{cr}$, which is quite reasonable. Note that the range of values for ξ_d inferred here is consistent with our earlier conclusion that $\xi_d \lesssim 1$, based on the lack of central brightening of the X-ray source.

Our analysis of the total scattering from the corona/wind gives us a handle of the intrinsic X-ray luminosity of the obscured central source. If 4U 2129+47 lies at a distance of d_{kpc} kiloparsecs, the observed flux in the 1–10 keV band is $L_{obs} = 1.1 \times 10^{34} d_{kpc}^2$ ergs s^{-1} (McClintock *et al.* 1982). This is small compared to the critical luminosity $L_{cr} \approx 1.3 \times 10^{37}$ ergs s^{-1}, so we expect the wind to be in Region C; in fact, the self-consistent solution of equation (3.9) bears this out. If the observable scattering is dominated by the wind at $\xi_d \sim 1$, then $L_{obs} = L_{sc}$(wind) and the intrinsic luminosity is

$$L = 5 \times 10^{35}\left[\frac{\Xi_0'}{f(\xi_d)}\left(\frac{M_x}{1.4\ M_\odot}\right)\right]^{1/2} d_{kpc}\ \mathrm{ergs\ s^{-1}}, \tag{3.25}$$

where we have assumed that the total luminosity is comparable to that in the 1–10 keV band. McClintock *et al.* (1982) obtained a similar result based on somewhat different reasoning. A lower limit on $f(\xi_d)$ is f_{is}, the attenuation factor in the inner shadowed zone (eq. [2.24]). Solving equations (2.24) and (3.25) with $\Xi' \sim 1$ for simplicity gives $f > 0.1 d_{kpc}^{-2/3}$, consistent with the value inferred below equation (3.24). In fact, f must be significantly greater than this since we have argued that the disk is thick enough to occult the inner shadowed zone. For $f(\xi_d)$ of order unity, the intrinsic luminosity in equation (3.25) is about 10–50 times the observed flux, for distances in the range $1.2 \lesssim d_{kpc} \lesssim 4$ kpc inferred from *UBV* photometry of 4U 2129+47 at minimum light (Thorstensen *et al.* 1979; McClintock, Remillard, and Margon 1981). We agree with McClintock *et al.* (1982) that the large modulated 3000–6000 Å optical flux can be ascribed to X-rays reprocessed in the photosphere of the occulting star. Provided $h_d(R_d)/R_d < 0.2$, more than a third of the stellar hemisphere facing the X-ray source will be illuminated by the full luminosity L, rather than by L_{sc} alone. An increase in the incident flux over L_{sc} by a factor ~ 10 is sufficient to produce the observed optical-to-(2–10 keV) X-ray ratio of 0.2 (corrected assuming $A_V = 1.5$) at maximum light, and this is readily available.

c) Polarization

Radiation scattered by a corona or wind may exhibit measurable linear polarization. If the disk axis is inclined at an angle i to the line of sight, then unpolarized radiation from the central source scattered in a ring of radius R_0 at height h above the midplane of the disk will acquire a net fractional polarization given by

$$\Pi_{sc} = \frac{\sin^2 i[1 - 2(h/R_0)^2]}{2[(1 + 2(h/R_0)^2] + [1 - 2(h/R_0)^2]\sin^2 i}, \tag{3.26}$$

where the electric vector is parallel to the projected disk axis (apparent minor axis) when Π_{sc} is positive, and parallel to the projected disk surface (major axis) when Π_{sc} is negative. Note that Π_{sc} vanishes and changes sign when $(h/R_0)^2 = \frac{1}{2}$. For an optically thin corona or wind, the observed fractional polarization of scattered radiation and its direction are obtained by weighting the emissivity j_{sc} (cf. § III*a*) of each ring by Π_{sc}, and integrating. If optical depth effects are important along the observer's line of sight ($\tau_{ob} \gtrsim 1$), then the calculation is more complicated, but provided that the half of the ring toward the observer is relatively unobscured, the effect of obscuring the remainder of the ring will not significantly affect the net polarization.

For a corona confined to a thin disk ($h/R_0 \ll 1$), the polarization of the scattered light is relatively large unless the disk is nearly face-on: the maximum value $\Pi_{sc} = \frac{1}{3}$ occurs for $i = 90°$, the average value is $\Pi_{sc} = 3/11$ at $i = 60°$, and the probability that $\Pi_{sc} < 0.1$ is only 0.12. As discussed in § III*a*, the scattering occurs primarily in the inner corona at $R_0 \sim R_{ia}$ and in the wind; since the former is geometrically thin whereas the latter includes

scattering at $h/R_0 > 2^{-1/2}$ where the polarization is opposite to the low-altitude value, we expect that the observed polarization will be dominated by scattering in the inner corona. If the central source is visible, then the observed continuum polarization Π_{obs} will be reduced from Π_{sc} by L_{sc}^{obs}/L. Reference to equation (3.20) shows that for a thin edge-on disk with a visible central source

$$\Pi_{obs} \approx 0.03 \left[\frac{T_{IC8}(L/L_E)}{\Xi'_{h,min}\epsilon_{-1}} \right]^{1/4} . \tag{3.27}$$

This estimate also should apply to disks with $i < 90°$ provided that they are not nearly face-on.

Quasars. The value of the continuum polarization predicted by equation (3.27) is inconsistent with the results of optical and infrared polarimetry of quasars and Seyferts, reviewed by Angel and Stockman (1980). While they identify a class of active galaxies and quasars which are highly polarized, the directions and magnitudes of polarization in these objects are highly variable, and presumably arise from effects other than scattering. Optically selected quasars which show steady polarization have $\Pi_{obs} \lesssim 0.5\%$ (Stockman and Angel 1978) whereas radio selected quasars have $\Pi_{obs} \sim 1\%$ (Stockman, Angel, and Miley 1979).

Nevertheless, there is no reason to abandon the idea that the small observed polarizations arise from electron scattering in a wind or corona, and indeed two pieces of evidence support this point of view. First, fractional polarizations in quasars and type I Seyfert galaxies appear to be wavelength independent (as one would expect for electron scattering). This contrasts with type II Seyferts, in which the polarization is probably due to scattering by dust (Angel and Stockman 1980). Second, Stockman, Angel, and Miley (1979) find that the polarization direction in quasars tends to be aligned with the axis of extended radio structure. Since extended radio sources are believed to be collimated along a rotation axis within the inner few parsecs of the nucleus (Rees, Begelman, and Blandford 1981), one would expect the radio structure to lie parallel to the accretion disk axis. Scattering off a corona and inner regions of the wind would produce polarization in the same direction, as observed.

There are a number of reasons why the observed polarization could be smaller than that predicted for a thin, Compton-heated corona: (1) *Strong heating of the corona* by, for example, tangled magnetic fields, so that $T_h \gg T_{IC} \sim 10^8$ K (Liang and Thompson 1979). Our estimate of the scattered luminosity does not apply to such coronae, and it is possible that L_{sc} is smaller in that case. A very hot corona would be much thicker than a Compton-heated corona, and the larger h/R_0 reduces the polarization (eq. [3.26]). (2) *Extension of the optical and infrared source* over a region larger than $R_{ia} \sim 2 \times 10^{16}(L_{46}M_8)^{1/2}$ cm. This is possible in objects with steady polarization because variability timescales at optical and infrared frequencies in such objects do not require the sources to be smaller than 10–$100R_{ia}$. X-ray emission from these objects may well show greater variability, which would indicate a correspondingly smaller source and higher degree of polarization. (3) *Lack of a clear line of sight* from the X-ray source to the disk photosphere at $R \sim R_{ia}$, due, for example, to lack of disk flare or to irregularity in the disk surface caused by gravitational instability. (4) *A very massive central object.* Then Π_{obs} would be reduced to 1%, comparable to that observed for quasars with extended radio structure, for $L/L_E \sim 10^{-2}$, which requires $M \sim 10^{10}\ M_\odot$ for $L \sim 10^{46}$ ergs s^{-1}.

Binary X-ray sources. A number of authors have pointed out the importance of X-ray polarimetry as a diagnostic of the parameters of binary X-ray sources (Angel 1969; Rees 1975; Lightman and Shapiro 1975, 1976), and observations of polarization of Cyg X-1, Cyg X-2, and Cyg X-3 at the several percent level have been reported by Long, Chanan, and Novick (1980). X-rays emitted from an opaque accretion disk in which electron scattering exceeds true absorption can be polarized by up to 12% in the plane of the disk (Chandrasekhar 1960), while those emitted from an optically thin disk can be polarized along the axis of the disk. X-rays emitted from a magnetized neutron star can show polarizations up to 75% (Rees 1975).

X-ray polarization due to the emission process can be distinguished in principle from that due to scattering in the corona by time-resolved polarimetry of eclipsing X-ray sources. The coronal scattering which we have analyzed occurs at a radius $\sim R_{ia}$, much larger than the radius at which the X-rays are emitted by an accreting neutron star or black hole. For an eclipsing system, $\sin i = O(1)$ and the X-ray polarization should be of order 30% as the corona emerges from eclipse but prior to the appearance of the central source. (This result could be altered if the emitted X-rays are highly polarized or if scattering in the atmosphere of the optical companion is important.) In fact, sources with $\sin i \sim 1$ may be permanently "eclipsed" by the corona and have a steady polarization much greater than 10%; this can occur if the corona at R_{ia} is visible but the central source is hidden behind the opaque inner corona. If the accretion disk blocks our view of the inner corona as well, as we have argued in the case for 4U 2129+47, then substantial polarization should still be present, although the thickness of the scattering region would reduce the polarization well below 30%. Polarimetry of 4U 2129+47 and 4U 1822−37 would provide valuable information on the geometry of the outer corona and wind.

IV. LINE EMISSION FROM THE DISK

An optically thick accretion disk radiating from within produces absorption lines, not emission lines. However, if the same disk is irradiated by X-rays and UV radiation from without, then a "chromosphere" can be produced

(Schwarzenberg-Czerny 1982) which converts some fraction of the absorbed energy into emission lines. A particular example of this process has been studied by Jones and Raine (1980), who analyzed scattering onto a disk from a wind originating at small radii ($\xi \lesssim 10^{-3}$); the wind was driven by radiation pressure associated with supercritical accretion, a possibility we excluded by our assumption that $L \ll L_E$. They ignored the effects of the corona produced by the scattered radiation, but our analysis of the radiative transfer is readily modified to cover their problem as well.

Line emission from irradiated slabs of gas has been extensively studied in connection with the broad emission line regions of quasars (Kwan and Krolik 1981 and references therein), and at the densities inferred for this problem ($n_e \lesssim 10^{10}$ cm^{-3}) this fraction is of order unity. In the case of X-rays reprocessed by the companion star in an X-ray binary, however, the densities are much greater and the fraction is small (London, McCray, and Auer 1981). Since the photospheres of the accretion disks we are studying span a broad range of densities, we shall first determine the conditions required to produce detectable emission lines. Accretion disks in bright binary X-ray sources are not promising sources of emission lines, but those in cataclysmic variables and quasars are.

a) Line Emission Efficiency

Consider the surface of a slab of gas exposed to an internally generated flux of radiation F_d at an effective temperature T_d, and to an external ionizing flux $F_{\rm ext}^{\rm ion}$. In our applications, this slab is a part of an accretion disk, but it could equally well be one of the gas clouds hypothesized to produce broad emission lines in quasars. The external flux induces the gas near the surface—in the "chromosphere"—to produce emission lines. Let F_l be the flux in emission line l and let

$$\eta_l \equiv F_l/F_{\rm ext}^{\rm ion} \tag{4.1}$$

be the efficiency with which external ionizing flux is converted into that line. [Following Krolik, McKee, and Tarter 1981 (KMT), we adopt the convention that $F^{\rm ion}$ includes radiation between 1 and 10^3 Ryd.] At low values of $F_{\rm ext}^{\rm ion}$, such as those normally considered in studies of quasar emission lines, η_l has a value η_{l0} which depends on the ionization parameter Ξ_0'; for permitted lines, η_{l0} varies weakly with density, depending on whether forbidden lines are collisionally suppressed. In Kwan and Krolik's (1981) standard model, $\eta_{l0} \approx (0.2, 0.14, 0.1)$ for (Lyα, C IV λ1549, Hα).

At high values of $F_{\rm ext}$, however, we have $\eta_l \ll \eta_{l0}$ since the flux in the line cannot exceed the blackbody limit

$$F_{lm} = \pi[B_\nu(T_{\rm ex}) - B_\nu(T_d)]\Delta\nu_{\rm em}\,, \tag{4.2}$$

where $B_\nu(T_{\rm ex})$ is the Planck function evaluated at the excitation temperature $T_{\rm ex}$ of the line and $\Delta\nu_{\rm em}$ is the local line width. [If the continuum is not a blackbody, then $B_\nu(T_d)$ is to be interpreted as the continuum flux evaluated at frequency ν.] Forbidden lines may never reach this limit because they may be optically thin. Note that the observed line width $\Delta\nu_{\rm obs}$ will generally be much greater than $\Delta\nu_{\rm em}$ due to rotational broadening. Detailed calculations would be required to determine F_{lm} accurately; it depends on the depth at which the external flux is absorbed, on the optical depth in the line, and on the efficiency of collisional thermalization. The essence of the situation can be described with a simple estimate: for Hα with $T_{\rm ex} = 10^4$ K, $B_\nu(T_d) \ll B_\nu(T_{\rm ex})$, and $\Delta\nu_{\rm em} = 80$ km s^{-1} (corresponding to an optical depth of about 10^4), we find $F_{lm} = 6 \times 10^7$ ergs cm^{-2} s^{-1}. This value varies by only a factor of a few as $T_{\rm ex}$ and the optical depth vary over a range of plausible values.

There is thus a critical value of the external flux, namely $F_{\rm ext}^{\rm ion} = F_{lm}/\eta_{l0}$, above which the fraction of the external flux that can be reprocessed into the usual strong emission lines such as Hα is reduced, and the fraction that is reprocessed into continuum radiation is increased. This in turn defines a critical radius $\xi_{\eta 0}$ given by

$$\eta_{l0}\, F_{\rm ext}^{\rm ion}(\xi_{\eta 0}) = F_{lm}\,. \tag{4.3}$$

Outside $\xi_{\eta 0}$, the flux $F_{\rm ext}^{\rm ion}$ is low and $\eta_l = \eta_{l0}$; inside $\xi_{\eta 0}$, the efficiency η_l drops as $(F_{\rm ext}^{\rm ion})^{-1}$ since $F_l \approx F_{lm}$ (see eq. [4.1]). For permitted lines we make the approximation

$$\frac{1}{F_l} = \frac{1}{F_{lm}} + \frac{1}{\eta_{l0}\, F_{\rm ext}^{\rm ion}}\,, \tag{4.4}$$

which reduces to the correct values at $\eta_{l0}\, F_{\rm ext}^{\rm ion} \gg F_{lm}$ and $\ll F_{lm}$. Then we can evaluate η_l as

$$\eta_l \approx \frac{\eta_{l0}}{1 + F_{\rm ext}^{\rm ion}(\xi)/F_{\rm ext}^{\rm ion}(\xi_{\eta 0})}\,. \tag{4.5}$$

Since the ionization parameter is fixed at $\Xi_0' = 4\pi J_{\rm ext}/p_0\, c$, the density at $\xi_{\eta 0}$ is determined to be

$$n_{\eta 0} = 1.05 \times 10^9 \left(\frac{4\pi J_{\rm ext}}{F_{\rm ext}^{\rm ion}}\right) \frac{F_{lm8}}{\eta_{l0}\, T_4\, \Xi_0'}\ {\rm cm}^{-3} \tag{4.6}$$

using equation (4.3), where T_4 is the gas temperature in units of 10^4 K.

Note that since $F_{\rm ext}^{\rm ion} \propto n$ for fixed Ξ_0' [and fixed $T_4^{-1}(4\pi J_{\rm ext}/F_{\rm ext}^{\rm ion})$], equation (4.5) can be written in the following form:

$$\eta_l = \frac{\eta_{l0}}{1 + n/n_{\eta 0}} . \tag{4.7}$$

Hence in this case permitted lines are suppressed at high densities just as forbidden and semiforbidden lines are. Interestingly enough, the critical density $n_{\eta 0}$ for permitted lines in equation (4.6) is of the same order as the critical density for the semiforbidden line C III] λ1909, a strong line in quasar spectra. Equation (4.7) allows for optical depth in the continuum as well as for collisional deexcitation of the line. On the basis of a detailed analysis, Mathews, Blumenthal, and Grandi (1980) concluded that the emissivity of hydrogen emission lines is curtailed above a density of $\sim 10^{10}$ cm^{-3}, consistent with our estimate from first principles.

Our analysis of radiative transfer and scattering in the corona (§ II, § III*a*) shows that there are two contributions to the ionizing external flux $F_{\rm ext}^{\rm ion}$: direct attenuated irradiation from the central source

$$F_{\rm irr}^{\rm ion} = \frac{L^{\rm ion}}{4\pi R_0^2} f \cos\theta_i , \tag{4.8}$$

and radiation scattered by the corona

$$F_{\rm sc}^{\rm ion} = 2\pi S_\perp^{\rm ion} \tag{4.9}$$

$$= \frac{L^{\rm ion}}{4\pi R_0^2} \frac{k_\tau(\xi/2)^{1/2}}{(1 + 2k_\tau + \xi/\xi_{\rm ia})} . \tag{4.10}$$

Here θ_i is the angle of incidence relative to the normal at the disk surface and $S_\perp$ is the scattered intensity normal to the disk (eq. [3.11]); in evaluating $F_{\rm sc}$ we have used the fact that the vertical scattering optical depth $\tau_\perp$ is small. Correspondingly, we have

$$\frac{4\pi J_{\rm ext}}{F_{\rm ext}^{\rm ion}} = \begin{cases} \dfrac{1}{\cos\theta_i} \dfrac{F_{\rm irr}}{F_{\rm irr}^{\rm ion}} & \text{(4.11a)} \\ (\ln \tau_\perp^{-1}) \dfrac{F_{\rm sc}}{F_{\rm sc}^{\rm ion}} & \text{(4.11b)} \end{cases}$$

for the factor in $n_{\eta 0}$ (eq. [4.6]) for the cases of direct irradiation and scattering, respectively.

The normalized radius of the point in the disk at which $F_{\rm irr}^{\rm ion}$ equals the critical value for line suppression F_{lm}/η_{l0} is denoted $\xi_{\eta \rm irr}$; equations (I2.7), (4.3), and (4.8) yield

$$\xi_{\eta \rm irr} = 3.4 \times 10^4 T_{\rm IC8} \left[\frac{\eta_{l0}}{F_{lm8}} \left(\frac{L^{\rm ion}}{L_{\rm E}} \right) \left(\frac{M_\odot}{M} \right) f \cos\theta_i \right]^{1/2} . \tag{4.12}$$

The corresponding critical radius for the scattered radiation is

$$\xi_{\eta \rm sc} = 790 T_{\rm IC8} \left[\frac{\eta_{l0}}{F_{lm8}} \left(\frac{L^{\rm ion}}{L_{\rm E}} \right)^{3/2} \left(\frac{L}{L^{\rm ion}} \right)^{1/2} \left(\frac{M_\odot}{M} \right) \frac{1}{(k_\tau \Xi'_{h,\min} \epsilon_{-1})^{1/2}} \right]^{2/5} , \tag{4.13}$$

where we have assumed $\xi_{\eta \rm sc} > \xi_{\rm ia}$. Then, since $F_{\rm ext}^{\rm ion} = F_{\rm irr}^{\rm ion} + F_{\rm sc}^{\rm ion}$, we have

$$\xi_{\eta 0} \approx \max (\xi_{\eta \rm irr}, \xi_{\eta \rm sc}) \tag{4.14}$$

as the radius inside which line emission is suppressed. One can show that $\xi_{\eta 0}$ is almost always outside the inner attenuation zone (i.e., $\xi_{\eta 0} > \xi_{\rm ia}$). Indeed, for stellar accretion disks $\xi_{\eta 0}$ is almost always greater than unity and η_l is less than η_{l0} over most of the disk. Inside $\xi_{\eta 0}$, the radius is related to the efficiency by

$$\xi(\eta_l) \approx \max \begin{cases} \xi_{\eta \rm irr} \left(\dfrac{\eta_l}{\eta_{l0}} \right)^{1/2} & \text{(4.15a)} \\ \dfrac{\xi_{\eta \rm sc} (\eta_l/\eta_{l0})^{2/5}}{1 + \{[(1 + 2k_\tau)\xi_{\rm ia}/\xi_{\eta \rm sc}](\eta_{l0}/\eta_l)^{2/5}\}^{2/3}} , & \text{(4.15b)} \end{cases}$$

where the scattering expression (4.15b) is based on an approximate solution of equation (4.10).

The suppression of the emission lines inside $\xi_{\eta 0}$ is reflected in the line profile. In a Keplerian disk, the orbital velocity at $\xi(\eta_l)$ is

$$v(\eta_l) = 1.16 \times 10^8 [T_{\rm IC8}/\xi(\eta_l)]^{1/2} \text{ cm s}^{-1} . \tag{4.16}$$

A line with a flux F_l which varies as ξ^{-m} has a profile

$$\begin{aligned} L_{lv} &\propto v^{2m-5} \quad (m < \tfrac{5}{2}) \\ &\propto \ln v/v_{\max} \quad (m = \tfrac{5}{2}) \\ &\propto \text{const} \quad (m > \tfrac{5}{2}) , \end{aligned} \tag{4.17}$$

where $v_{\max}$ is the maximum orbital velocity v and where we assumed $v \ll v_{\max}$. For $\xi < \xi_{\eta 0}$, the line flux is approximately constant ($m = 0$) so that the profile is sharply cut off, $L_{lv} \propto v^{-5}$.

b) X-Ray Binaries and Cataclysmic Variables

For stellar accretion disks, equations (4.12) and (4.13) indicate that the radius at which the emission lines attain their full efficiency η_{l0} is almost always at $R_0 \gg R_{\rm IC}$ and hence beyond the edge of the disk. A necessary condition that the lines be detectable is that the efficiency η_l exceed some threshold which depends on the sensitivity of the detector for broad ($\Delta v \sim 10^3$ km s^{-1}), weak emission lines. For example, a line which is 3% above the continuum over a bandwidth $\Delta v/c \sim 1/300$ has a fractional equivalent width $W_\lambda/\lambda \approx 10^{-4}$. To produce such a line, η_l must exceed W_λ/λ because the observed continuum may include radiation from regions not contributing line emission. Note that at $\eta_l = 10^{-4}$, the effective temperature of the external flux is $T_{\rm eff} = (F_{lm}/\sigma\eta_l)^{1/4} = 11{,}500 F_{lm8}^{1/4}$ K. If this is the minimum detectable line, then the disk must extend beyond the radius at which $\eta_l = 10^{-4}$. For example, a directly irradiated disk with $M \sim 1\ M_\odot$ must satisfy

$$R_d > R_{\rm IC}\,\xi(\eta_l = 10^{-4}) \approx 1.0 \times 10^{12}[(L^{\rm ion}/L_{\rm E})(10 f \cos\theta_i) F_{lm8}^{-1}]^{1/2} \text{ cm} , \tag{4.18}$$

from equations (4.12) and (4.15a). This is impossible for a bright binary X-ray source with $L^{\rm ion}/L_{\rm E} \gg 10^{-2}$ unless $f \cos\theta_i \ll 1$. Alternatively, if the condition for detecting a line is known as a lower limit on the line luminosity L_l, we have $L_l < 2\pi R_d^2 F_{lm}$, or

$$R_d > 4 \times 10^{10}(L_l/10^{30} \text{ ergs s})^{1/2} F_{lm8}^{-1/2} \text{ cm} . \tag{4.19}$$

One example of an X-ray binary with an emission line attributed to the disk is 2A 1822−371 (4U 1822−37), in which He II λ4686 has been seen with an equivalent width of 2.5 Å (Charles, Thorstensen, and Barr 1980; Cowley, Crampton, and Hutchings 1982). Strong far-UV emission lines have also been detected, but their source is not clear (Mason and Córdova 1982*a*). For He II λ4686, we estimate $L_l = 1.2 \times 10^{30} d_{\rm kpc}^2$ ergs s^{-1}. For a total mass of 1.3 $M_\odot$ (Cowley, Crampton, and Hutchings 1982), the Paczyński-Smak radius $R_{\max}$ (eq. [I4.20]) for this disk is about 7×10^{10} cm, so equation (4.19) leads to an upper limit of $1.6 F_{lm8}^{1/2}$ kpc for the distance to this object and $5 \times 10^{35} F_{lm8}$ ergs s^{-1} for the observable X-ray luminosity. These numbers are in excellent agreement with recent observations by Mason and Córdova (1982*b*), which suggest that the source is closer and fainter than had previously been thought. Although F_{lm} may be somewhat greater than 10^8 ergs cm^{-2} s^{-1} for a high-excitation line such as He II λ4686, we conclude that 2A 1822−371 has a relatively low observable luminosity. Since this source exhibits extended eclipses like those of 4U 2129+47 (§ III*b*), its intrinsic luminosity may be an order of magnitude greater than the observed luminosity due to shielding by the disk.

A second, better-known example of an X-ray binary with disk emission lines is Sco X-1 (Cowley and Crampton 1975; Crampton *et al.* 1976), which is at an uncertain distance of order 0.3–1 kpc. The dereddened luminosity in He II λ4686 is $L_l \sim 3 \times 10^{31} d_k^2$ ergs s^{-1}. Since $a \sin i$ is observed to be 6×10^{10} cm and $\sin i \gtrsim \frac{1}{2}$ for plausible masses (Cowley and Crampton 1975), the maximum size of the disk is comparable to that in 2A 1822−371. Equation (4.19) then leads to the distance estimate $d_k \lesssim 0.3 F_{lm8}^{1/2} \lesssim 1$, consistent with previous estimates. The small ratio of optical to X-ray luminosity ($\sim 10^{-3}$) implies a small value for $f \cos\theta_i$ as well: in the outer region of the disk, most of absorbed X-rays will be reprocessed into optical radiation, so $L_{\rm opt}/L_x = f h_d/R_d \approx f \cos\theta_i \sim 10^{-3}$.

Cataclysmic variables have $L/L_{\rm E} \lesssim 10^{-4}$ and can readily produce lines of detectable equivalent width according to equation (4.19). Since $L/L_{\rm E}$ is small, the effects of scattering are weak and $f \sim 1$. The density of the emitting gas near the edge of the disk is

$$n = \frac{8 \times 10^{13} L_{34}^{\rm ion}}{T_4\, \Xi_0'\, R_{d10}^2} \text{ cm}^{-3} . \tag{4.20}$$

An alternative to the chromospheric model for emission lines from accretion disks has been developed by Williams (1980), who showed that the outer regions of a low mass accretion disk are semitransparent in the continuum and therefore produce emission lines due to viscous dissipation in the disk. High-excitation lines, such as those of helium, cannot be produced by this mechanism. Our estimate for the maximum η_l applies to this model as well. As we shall see in § V below, the external flux from the central source and inner regions of the disk is often greater than the locally produced flux and hence dominates the excitation of the emission lines.

c) *Quasars, Seyferts, and BL Lac Objects*

The broad emission lines from quasars and Seyfert galaxies are generally attributed to reprocessing of continuum radiation from a central source by myriads of small, opaque, fast-moving clouds. In our notation, the line luminosity from such clouds is $L_l = \eta_l CL$, where C is the covering factor of the clouds. The lack of absorption in quasars indicates $C \lesssim 0.1$ (Oke and Korycansky 1982), so the large observed line luminosities require $\eta_l \sim \eta_{l0}$. The size of the emission line region $R_{\rm em}$ must exceed $\xi_{\eta 0} R_{\rm IC} = \xi_{\eta \rm irr} R_{\rm IC}$, or

$$R_{\rm em} > 2.8 \times 10^{18} (\eta_{l0} L_{46}^{\rm ion}/F_{lm8})^{1/2} \text{ cm} . \tag{4.21}$$

This confirms the usual simple estimate, which is based on the requirement that the density be low enough that C III] λ1909 not be collisionally suppressed; it is also consistent with detailed photoionization calculations (e.g., Kwan and Krolik 1981).

It is usually assumed that quasars and active galactic nuclei are powered by a central massive object with an accretion disk. If the disk is sufficiently large ($\xi > 0.1$, or $R > 10^{17} M_8 T_{\rm IC8}^{-1}$ cm) and is exposed to the central X-ray source, a strong wind will occur which can confine the emission-line clouds and thereby produce the two-phase emission line region envisioned by KMT. The ionization parameter in the wind is of order $\Xi'_{c,\rm max}$, which is comparable to, though somewhat larger than, the observed value. Either relative motion between the clouds and wind, or evaporation of the clouds by the hot ambient gas, would raise the cloud pressure and bring the cloud ionization into closer agreement with observation. In some cases, electron scattering in the wind could produce ultrabroad wings on the emission lines (Shields and McKee 1981).

The underlying accretion disk would also give rise to emission lines, which may be detectable. Since the surface of the disk has an ionization parameter Ξ'_0 between $\Xi'_{h,\rm min}$ and $\Xi'_{c,\rm max}$, it is automatically in the correct range of ionization (KMT). Straightforward application of the results developed above indicates that a significant fraction of the emission line flux in quasars could arise in the disk. In fact, in the inner shadowed zone, beyond $\xi_{\eta 0}$, the line flux $F_l = \eta_{l0} F_{\rm sc}$ varies as $r^{-5/2}$. In this case the line profile is approximately logarithmic, in rough agreement with observation (Capriotti, Foltz, and Byard 1980; see eq. [4.17]). There are several major objections to a disk providing most of the broad line emission, however: (1) The low observed optical polarization indicates that the division of quasar accretion disks into inner attenuation and inner shadowed zones is invalid for optical radiation, at least (§ III*c*). (2) Disks around massive black holes tend to be gravitationally unstable at radii $\gtrsim \xi_{\eta 0} R_{\rm IC}$, so the disk may be highly clumped and the effective area substantially reduced. (3) If the inner shadowed zone exists insofar as ionizing radiation is concerned, the permitted lines have their peak efficiency for $n \lesssim 10^{11}$ cm^{-3} [from eq. (4.6) with $\eta_{l0} \sim 0.1$ and $4\pi J/F_{\rm ext}^{\rm ion} \sim (\cos \theta_i)^{-1} \sim 10$], whereas C III] λ1909 has its peak efficiency only for $n \lesssim 3 \times 10^9$ cm^{-3}. Since n varies roughly as R_0^{-2} and hence as v^4, this difference in density translates into a velocity difference in excess of a factor 2. However, the observed profiles of the UV permitted lines are quite similar to those of C III] λ1909. (4) As Shields (1978) has pointed out, it it difficult to reconcile the profiles of the permitted lines with those of the forbidden lines at lower velocities, $\Delta v \sim 10^3$ km s^{-1}. Other difficulties, especially in matching the observed asymmetries in the line profiles, have been discussed by Mathews (1982).

For these reasons we do not claim that the bulk of the flux in each of the quasar emission lines arises in an accretion disk. Nonetheless, a portion of each line should arise in the disk, and it is a challenging observational problem to detect this portion. A line produced in the region where F_l has saturated at F_{lm} would be characterized by a large line width ($\Delta v \gtrsim 10^4$ km s^{-1}) and it would be subject to variability on a time scale of months, provided the continuum varies (Blandford and McKee 1982).

Seyfert galaxies and broad-line radio galaxies have substantially lower luminosities than quasars, and they may be radiating at well below the Eddington limit. For low luminosities, $L/L_{\rm E} \lesssim 10^{-3}$, some of the problems afflicting the accretion disk interpretation of the emission lines are ameliorated: in particular, the polarization is reduced to within the observed range (eq. [3.27]), and $\xi_{\eta 0}$ is reduced somewhat so that gravitational instability may be less of a problem. At these low values of $L/L_{\rm E}$, direct attenuated radiation dominates scattered radiation, so the line profile depends on the shape of the disk and the equivalent width is determined by the relative disk thickness h_d/R. We conclude that objects with low $L/L_{\rm E}$ should produce a larger fraction of their emission lines in a disk than those with high $L/L_{\rm E}$.

We end our discussion with a speculation on BL Lac objects, which are conjectured to be active galactic nuclei with relativistic beams oriented toward us (Blandford and Rees 1978). Accretion disks associated with these objects should produce weak permitted emission lines with a strength proportional to the (unknown) isotropic luminosity, well below the observed luminosity. If the disk is normal to the relativistic beam, then the lines should be relatively narrow. BL Lac objects are highly variable, but unfortunately it is not known if the isotropic luminosity is variable as well; if it were, they would be ideal candidates for reverberation mapping of the disk (Blandford and McKee 1982). Observation of line variability would be the best way of distinguishing these lines from the observed narrow lines, which are generally forbidden lines and hence are produced in low-density gas far from the central object.

V. CONTINUUM EMISSION FROM THE DISK

Viscous dissipation inside the disk produces a flux of radiation at the surface of $F_d = 2\pi J_d \propto R_0^{-3}$ (see eq. [2.10]), with an effective temperature

$$T_d = 2.60 \times 10^4 \left[\left(\frac{L}{L_E}\right)\left(\frac{M_\odot}{M}\right)\frac{1}{\epsilon_{-1}}\right]^{1/4}\left(\frac{T_{IC8}}{\xi}\right)^{3/4} \text{K} . \tag{5.1}$$

Radiation from the central source often produces a larger flux at the surface than this internally generated radiation, since most of the energy is released near the center. For direct attenuated radiation, about one-third of the incident radiation is absorbed (Cunningham 1976), so that the effective temperature is determined by

$$\sigma T_{irr}^4 \approx \frac{1}{3} F_{irr} = \frac{1}{3}\frac{Lf \cos\theta_i}{4\pi R^2} , \tag{5.2}$$

which gives

$$T_{irr} = 1.6 \times 10^5 \left[\left(\frac{L}{L_E}\right)\left(\frac{M_\odot}{M}\right) f \cos\theta_i\right]^{1/4}\left(\frac{T_{IC8}}{\xi}\right)^{1/2} \text{K} . \tag{5.3}$$

Hence, T_{irr} exceeds T_d for

$$\xi > 7.8 \times 10^{-4} T_{IC8}/(\epsilon_{-1} f \cos\theta_i) , \tag{5.4}$$

which comprises most of the disk unless the denominator is very small (as it is for a thin disk around a white dwarf, for example). For small values of $f \cos\theta_i$, scattered radiation F_{sc} may dominate F_{irr}, and expressions analogous to equations (5.2) and (5.3) can be easily obtained by setting $F_{sc} \approx 2\pi S_\perp$ and using equations (3.5) and (3.11).

The fact that the external flux F_{ext} exceeds the locally generated flux F_d over much of the disk has consequences for the appearance of the disk and for its structure (see Paper I). Numerical calculations of the emission from a disk, including heating of the outer parts by the hot inner parts, but with no corona, have been made by Cunningham (1976) and by Pacharintanakul and Katz (1980). A disk radiating like a blackbody with $F \propto \xi^{-m}$ has a spectral luminosity

$$L_\nu \approx \left[\frac{2\Gamma(8m/3)}{3m}\right]\frac{4\pi R_{IC}^2 \sigma T(1)^4}{[kT(1)/h]}\left[\frac{h\nu}{kT(1)}\right]^{-(8-3m)/m} , \tag{5.5}$$

where $\Gamma(8m/3)$ is the gamma function and $T(1)$ is the effective temperature of the disk evaluated at $\xi = 1$. For the case of no irradiation, we have $F = F_d \propto \xi^{-3}$ and we recover the usual result $L_\nu \propto \nu^{1/3}$ (Lynden-Bell 1969). When the external irradiation is dominant, however, the spectrum is quite different:

$$\begin{aligned} L_\nu &\propto \nu^{-7/5} \quad \text{(inner attenuation zone)} \\ &\propto \nu^{-1/5} \quad \text{(inner shadowed zone)} \\ &\propto \nu^{-1} \quad (f \cos\theta_i = \text{const}) , \end{aligned} \tag{5.6}$$

where we have assumed that a fixed fraction of the incident flux is reemitted as thermal continuum. In the inner attenuation zone and inner shadowed zone, the radiation reaching the surface of the disk (i.e., below the cool corona) is primarily scattered radiation, as discussed at the end of § II*b*; the spectral index then follows from equation (3.11), which gives $m = (3/2, 5/2)$ for the two zones. In the outer part of the disk, direct attenuated radiation may dominate the incident flux, and then the spectral index depends directly on the uncertain shape of the disk through the radial dependence of $\cos\theta_i$. On the other hand, if scattered radiation dominates the flux, then we expect $2 \lesssim m \lesssim 3$ from equation (3.5), corresponding to $-1 \lesssim d \ln L_\nu / d \ln \nu \lesssim \frac{1}{3}$. Measurement of the continuum spectrum of the disk thus provides a sensitive test for the structure of the disk and corona, which together determine F_{ext}. In particular, when F_{ext} exceeds F_d, the spectrum often falls with frequency, in contrast to the canonical rising spectrum. In applying these results, it must be borne in mind that we have assumed that the disk is opaque in the continuum to both the internal and external fluxes, which is invalid in the outer regions of low mass disks (Williams 1980). Edge effects, which we have ignored, would modify the emitted spectrum as well.

Reprocessing by a disk has been suggested to account for the high ratio of UV to X-ray flux observed in Sco X-1 and Cyg X-2 (Chiappetti *et al.* 1983). In Cyg X-2, these authors find that the luminosity between 1000 Å and 5000 Å is about 1/15 of the X-ray luminosity, which exceeds that expected from a standard accretion disk by a factor ~ 10. The slowly rising spectrum, $d \ln L_\nu / d \ln \nu = 0.2 \pm 0.2$, corresponds to $m = 2.9 \pm 0.1$. This could arise in a directly irradiated disk in which $f \cos\theta_i$ declines with radius; in a luminous source such as Cyg X-2, scattered

radiation may also be important in heating the disk. If we suppose that direct attenuated radiation dominates the heating of the disk and set $m = 3$, then the disk luminosity below a frequency ν is

$$\frac{L(<\nu)}{L} = 0.08 f(1) \cos \theta_i(1) \left[\frac{h\nu}{kT(1)}\right]^{4/3}, \tag{5.7}$$

where we have used equations (5.2) and (5.5) and where $f(1)$ and $\theta_i(1)$ are evaluated at $\xi = 1$. Adopting a distance of 8 kpc and a mass $M_x = 1.4\ M_\odot$ (Cowley, Crampton, and Hutchings 1979), and setting $T_{IC} \approx 10^7$ K and $L/L_E \approx \frac{1}{3}$ (Parsignault and Grindlay 1978), we find

$$T_{irr} = 3.5 \times 10^4 [f(1) \cos \theta_i(1)]^{1/4} \xi^{-3/4} \text{ K}. \tag{5.8}$$

The requirement that the disk luminosity for $\lambda > 1000$ Å be $L/15$ then gives $f(1) \cos \theta_i(1) = 0.04$, a plausible value. Tidal truncation limits the disk to a radius $R_{max} \approx 4 \times 10^{11}$ cm, somewhat smaller than truncation by a Compton-heated wind. Since $R_{IC} = 1.4 \times 10^{11}$ cm, the temperature at the edge of the disk is $T_{irr} = T(1)(R_d/R_{IC})^{-3/4} = 7000$ K, which is low enough to account for the near-UV portion of the spectrum.

VI. SUMMARY

There are a variety of possible geometric arrangements which can result in the formation of a Compton-heated corona and wind above an accretion disk. We have focused on the case in which the source of hard radiation is located in a compact region at the center of the disk; radiation from this source can reach the photosphere of the opaque disk because the photosphere "flares" with radius.

Analyzing this configuration self-consistently, we find the intensity at the base of the flow, and hence the pressure and density, may be strongly affected by attenuation. This is particularly true of rays which traverse the inner part of the corona, where the initially more intense flux of incident radiation is reduced to a flux comparable with that arising locally in the disk. The competition between Compton heating by the attenuated incident flux and cooling by the locally emitted radiation regulates the optical depth, and hence the density, of the hottest layer of the inner corona, and results in the establishment of a "cool corona," sandwiched between the hot layer and the underlying disk. Radiation scattered down onto the disk from the hot corona has a small effect on conditions near the base of the hot corona, except for L close to L_E; but scattered radiation may govern the thermal balance of the cool corona and the disk surface.

Depending on the extent of disk flare, much of the disk at larger radii may lie in the shadow of this "inner attenuation zone," with consequent reduction in the densities and mass loss rates in coronae and winds. Nevertheless, it is important to note two circumstances in which attenuation may be relatively unimportant over the entire disk. First, at very low luminosities ($L \lesssim 5 \times 10^{-4} L_E$) the size of the inner attenuation zone shrinks to the point where it no longer causes any attenuation; second, if the inner radius of the irradiated disk lies outside the radius associated with the inner attenuation zone, then the zone simply does not exist. The latter situation could occur, for example, if the accretion disk terminates at the magnetopause of a magnetized neutron star or at the surface of a white dwarf. Even where attenuation is important in determining conditions near the base of the flow, we find that most of the heating occurs sufficiently far above the disk that the line of sight to the central source is transparent. Consequently, the basic classification of solutions in terms of the competition between heating and gravity (§ II and Fig. I.1) is intact.

Incorporating these results into the dynamical analysis of Paper I, we discussed some of the observational signatures of Compton-heated coronae and winds. Largely, these can be derived from the scattering properties of the heated gas distribution, which we have mapped for flow above a flaring disk. In a steady source with arbitrary orientation, it would be difficult to separate the scattered from the direct radiation, although if the disk were nearly edge-on then the compact source and even the inner corona might be obscured from view. X-ray polarimetry should yield polarizations of a few percent for moderately inclined sources with the central source visible, and up to 10%–30% for edge-on sources with the nucleus obscured, provided the X-ray source is not intrinsically polarized. The electric vector of the radiation should point along the disk axis, the direction of which may be inferable independently from observations of radio structure. Direct measurements of scattered emission from a Compton-heated corona/wind may be obtained from time-dependent objects, such as eclipsing binaries where the extent and structure of the scattering region may be manifested in the light curve. We have shown how the light curves of the partially eclipsing binaries 4U 2129+47 and 4U 1822−37 can be interpreted in terms of Compton-heated coronae/winds, and have used our theory to infer the intrinsic luminosity of the obscured compact X-ray source in 4U 2129+47. One thing that Compton-heated winds *cannot* do is to create the very hard component of sources like Cyg X-1 and HZ Her through Comptonization of a softer central source. This would still require a hotter, nonthermally driven corona, as has been suggested by a number of authors (Liang and Price 1977; Liang and Thompson 1979; Payne and Eardley 1977). In quasars, an extended scattering atmosphere may be detected via a form of "reverberation mapping" (Blandford and McKee 1982). The polarization of radio-quiet quasars is less than that predicted by our theory,

suggesting that the source of the optical and infrared radiation is extended ($R > 10^{16} M_8$ cm) or that the disk does not flare.

Radiation striking the disk photosphere is reradiated in emission lines and in the continuum. The fraction of the incident ionizing radiation which is processed into lines decreases as the incident flux (and, at constant Ξ_0', the density) increases (see § IV); hence attenuation of the incident flux by the corona or wind can *aid* in the production of detectable lines. At the same time, the presence of a corona or wind *limits* line formation by scattering a certain minimal flux of hard radiation down to the disk, thereby setting a lower limit on the effective temperature of the photosphere. Our analysis of the emission-line luminosity provides a lower bound on the size of the accretion disk and an approximate upper bound on the distance to the source. Refinement of this technique could lead to reasonably accurate distance estimates to sources such as Sco X-1.

If disks in quasars and Seyfert galaxies extend out to sufficiently large radii, they ought to be efficient line emitters. Because of the grazing incidence of radiation from the nucleus and the attenuating effects of the corona, the minimum radius required for efficient line emission is smaller than the radius inferred for standard models of the broad emission line region, which consist of frontally illuminated clouds. Nevertheless, there are several observational objections to the disk providing all of the observed line emission in quasars, most notably the low value of optical and infrared polarization, and apparent profile similarities between lines which ought to come from different parts of the disk. Furthermore, estimates of the flare and surface area of the line-emitting region are on theoretically shaky grounds because naive application of standard accretion disk models to quasars yield disks which are vertically self-gravitating at the radii associated with line emission (Kolykhalov and Sunyaev 1982; Sakimoto and Coroniti 1981). We expect that instabilities in such disks may lead to clumping, making it difficult to estimate reliably the absorbed X-ray flux and line emission. (However, we do not expect clumping to substantially change the dynamical properties of the corona or wind, providing the flare of the disk as a whole is known.) We therefore suggest that disks provide only a fraction of the line emission in quasars; however, if lower luminosity objects (e.g., Seyferts and broad-line radio galaxies) contain comparably massive black holes and are merely radiating at $\lesssim 10^{-3}$ of the Eddington limit, then both the polarization and self-gravitation problems are ameliorated, and it becomes more plausible to suggest that the disk produces most or all of the line emission.

Absorbed radiation which is not channeled into lines will be reemitted as continuum, the flux of which may easily exceed that of continuum generated locally within the disk. This reprocessed continuum should be thermalized at roughly its effective temperature if the disk is opaque, and its spectrum may differ significantly from the $\nu^{1/3}$ spectrum characteristic of an optically thick accretion disk radiating from within (Lynden-Bell 1969). The spectral index depends sensitively on the manner in which the disk is illuminated and can provide a sensitive diagnostic of disk and coronal structure. In sources such as Cyg X-2, this reprocessed continuum may dominate the UV emission from the system (Chiappetti *et al.* 1983).

This work is an outgrowth of a project in collaboration with Greg Shields, and we thank him for many valuable discussions. We gratefully acknowledge a number of suggestions by Richard London, which significantly improved the paper. Helpful comments were also made by Roger Blandford and Anne Cowley. C. F. M. expresses his gratitude to the Sherman Fairchild Distinguished Scholars Program for supporting his stay at the California Institute of Technology during the inception of this work, and to Martin Rees for supporting his stay at the Institute of Astronomy in Cambridge where the work continued. The work of C. F. M. and M. C. B. is supported in part by the National Science Foundation under grants AST 79-23243 and AST 82-15456, and M. C. B. additionally acknowledges partial support from the Science Research Council of Great Britain.

APPENDIX A

SELECTED GLOSSARY OF FREQUENTLY USED SYMBOLS

F	Flux of radiation, measured near the source
F_d	Flux generated internally in the disk
$F_{\rm irr}$	Flux normal to the disk, directly from the source
$F_{\rm sc}$	Flux normal to the disk, scattered in corona/wind
$F_{\rm ext}$	$F_{\rm irr} + F_{\rm sc}$
$F^{\rm ion}$	Ionizing flux: 1 Ryd $< h\nu <$ 10^3 Ryd
F_l	Flux in emission line l
F_{lm}	Maximum F_l set by blackbody limit
f_Γ	Form factor for heating rate (eq. [I3.9])
$f_{\Gamma_0} \equiv f$	Attenuation factor (eq. [2.1]) = form factor for heating at base of corona/wind

f_d	Form factor for cooling by disk radiation (eq. [2.11]) = attenuation factor at the base of the hot corona in the inner attenuation zone
f_{is}	Attenuation factor in inner shadowed zone (eq. [2.24])
f_{sc}	Form factor for heating due to scattered radiation (eq. [2.29])
h	Height above midplane of disk
h_d	Height of disk photosphere above midplane, effective thickness of disk
h_c	Scale height of corona (eq. [2.6])
h_{hc}	Height at lower boundary of hot corona
J, J^{ion}	Mean intensity of radiation integrated over all frequencies, from 1–10^3 rydbergs
J_0	Mean intensity of radiation at base of corona/wind (eq. [2.1])
J_d	Mean intensity of radiation, emitted locally by disk (eq. [2.10])
j_{sc}	Local scattering emissivity (eq. [3.1])
k_τ	Defined eq. (2.19)
L, L^{ion}	Total luminosity, luminosity of ionizing radiation ($1 \leq h\nu \leq 10^3$ rydbergs)
L_E	Eddington limit
L_{cr}	Critical luminosity for wind parameter space (eq. [I2.12])
L_{sc}	Luminosity of scattered radiation
L^{obs}	Luminosity of observed portion of radiation
M	Mass at center of accretion disk
p_0	Gas pressure at base of corona/wind (eq. [2.2])
R_0	Radius in plane of accretion disk
R_{IC}	Radius at which Compton temperature equals escape temperature (eq. [I2.7])
R_{ia}	Radius of inner attenuation zone (eq. [2.23])
R_{is}	Boundary between inner and outer shadowed zones (eq. [2.26])
R_d	Outer radius of disk
R_t	Radius at which line of sight from observer most closely approaches compact X-ray source
R_{opt}	Radius of occulting star in X-ray binary
S	Surface brightness of scattered radiation (eq. [3.2])
$S_\perp$	Surface brightness of scattered radiation for face-on disk (eqs. [3.5] and [3.11])
$S_\parallel$	Surface brightness of scattered radiation for edge-on disk (eqs. [3.7] and [3.18])
s	Flare exponent (eq. [2.4])
T_h	Equilibrium temperature of hot phase
T_{IC}	"Inverse Compton temperature," at which Compton heating balances inverse Compton cooling (eq. [I2.4])
T_d	Effective temperature ($\approx$inverse Compton temperature) of radiation emitted locally by disk
z	Dimensionless height above disk photosphere $\equiv (h - h_d)/R_0$
Γ	Heating rate
ϵ	Efficiency of mass-to-energy conversion in the accretion flow = $10\epsilon_{-1}$
η_l	$\equiv F_l/F_{ext}^{ion}$: efficiency with which disk reprocesses incident ionizing flux into emission line l (eq. [4.1])
η_{l_0}	Value of η_l for unsaturated line, i.e., at low F_{ext}^{ion} and low n
θ_0	Spreading angle of scattered X-ray source (cf. Fig. 2*a*)
θ_i	Angle of incidence of incident rays on disk photosphere, measured relative to normal at disk surface
$\tilde{\mu}$	Mass ratio of compact X-ray source to total mass of binary
Ξ'	Ionization parameter; for a beam of radiation, ratio of radiation pressure to gas pressure (eq. [I2.1])
$\Xi'_{c,max}$	Maximum Ξ' allowing gas in cool phase
$\Xi'_{h,min}$	Minimum Ξ' allowing gas in hot phase
Ξ'_0	Ξ' at base of corona/wind (eq. [2.2])
ξ	$\equiv R_0/R_{IC}$ (eq. [2.8]); in general, $\xi_x = R_x/R_0$
ξ_G	ξ at which $h_c = h_d$; for $\xi > \xi_G$, $h_c > h_d$ (eq. [2.7])
ξ_{hc}	ξ at which $f_d = f_T$; hot corona exists outside ξ_{hc} (eq. [2.12])
ξ_{min}	ξ at which line of sight from source first enters corona (eq. [2.19])
ξ_{os}	Outer radius of shadowed zone
ξ_1	ξ at which line of sight through edge-on corona becomes optically thick (eq. [3.17])
$\xi_{\eta 0}$	ξ at which emission line from disk becomes saturated (eq. [4.3])
$\xi_{\eta irr}$	$\xi_{\eta 0}$ for case in which disk is directly irradiated by central source (eq. [4.12])
$\xi_{\eta sc}$	Same as $\xi_{\eta irr}$, except that irradiation is by radiation scattered in corona/wind (eq. [4.13])
τ_s	Optical depth along line of sight to source
$\tau_\parallel$	Characteristic optical depth, $\equiv n_e \sigma_T R_0$
$\tau_\perp$	Optical depth in corona/wind normal to disk
τ_{ob}	Optical depth along line of sight from observer to scattering point (eq. [3.2])
ϕ_{dIC}	Defined eq. (2.4)

APPENDIX B

ATTENUATION IN THE WIND

Consider a ray from the source of radiation which reaches the disk surface at R_0. At a radius R from the center it passes above the disk at a height zR given by

$$z = \phi_{d\mathrm{IC}}(\xi_0^s - \xi^s)\,, \tag{B1}$$

where in this Appendix $\xi = R/R_{\mathrm{IC}}$ and $\xi_0 = R_0/R_{\mathrm{IC}}$. Let $\tau(R, R_0)$ be the optical depth in the wind at a radius R on this ray. We wish to find the attenuation factor $f = f_{\mathrm{sh}} \exp[-\tau(R_0, R_0)] \equiv f_{\mathrm{sh}} \exp(-\tau_0)$, where f_{sh} is the attenuation factor due to shadowing, given by (2.24) if $f_{\mathrm{sh}} < 1$ and equal to unity otherwise.

We showed in § II that the optical depth high above the disk ($z \sim 1$) is small, so we need to consider only the region close to the surface of the disk. There the steady heating analysis of § III*d*, Paper I, is applicable, even in Region A. We approximate $y \approx 1$, $p^* \approx 1$, $\eta \approx 1$ and, from equation (I3.19),

$$T^{*3/2} \approx \tfrac{2}{5} z f_\Gamma = \tfrac{2}{5} z f_{\mathrm{sh}}\, e^{-\tau(R, R_0)}\,. \tag{B2}$$

(In this Appendix we assume the reader is familiar with the detailed results of Paper I, and we do not redefine symbols introduced there.) Then one finds that the electron scattering opacity κ at a point (R, z) is given by

$$\kappa(R, z) = \kappa(R_{\mathrm{IC}}, 1)\, \frac{e^{-\tau_0 + \tau(R, R_0)/2}}{\xi^{4/3 - \nu/2} z^{1/2}}\,, \tag{B3}$$

where the constant $\kappa(R_{\mathrm{IC}}, 1)$ is given by

$$\kappa(R_{\mathrm{IC}}, 1) = \frac{0.048}{\Xi_0'} \left(\frac{L}{L_{\mathrm{cr}}}\right)^{1/3} \left(\frac{\dot{m}_{\mathrm{IC}}^* f_{\mathrm{sh}}}{T_{\mathrm{IC8}}}\right)^{1/2}\,. \tag{B4}$$

Substituting this into the identity

$$\frac{d}{dR}\, e^{-\tau(R, R_0)/2} = -\frac{1}{2}\, \kappa(R, z) e^{-\tau(R, R_0)/2}$$

and integrating, we obtain an integral equation for τ_0:

$$e^{-\tau_0/2} = 1 - \frac{1}{2}\, \kappa(R_{\mathrm{IC}}, 1) \int_1^{\xi_0} \frac{d\xi}{\xi^{4/3 - \nu/2} z^{1/2}}\, e^{-\tau_0}\,. \tag{B5}$$

An upper limit on τ_0 can be found by setting

$$e^{-\tau_0} = \frac{1}{1 + a\xi_0^n} \tag{B6}$$

and then placing an upper bound on a. If the attenuation begins at ξ_1, this gives

$$a < \frac{1}{2}\, \kappa(R_{\mathrm{IC}}, 1) \int_{\xi_1}^{\xi_0} \frac{d\xi}{\xi^{4/3 - \nu/2 + n} z^{1/2}}\,, \tag{B7}$$

or, by using equation (B1),

$$a < \frac{\pi}{2s}\, \frac{\kappa(R_{\mathrm{IC}}, 1)}{\phi_{d\mathrm{IC}}^{1/2}}\,, \tag{B8}$$

where we have assumed $\xi_0 \gg \xi_1$. The requirement that a not vary as a power of ξ implies

$$n = -\tfrac{1}{3} + \tfrac{1}{2}\nu - \tfrac{1}{2}s = -(\tfrac{2}{3} + \tfrac{1}{2}s, \tfrac{1}{3} + \tfrac{1}{2}s, \tfrac{1}{2}s)$$

for Regions A, B, and C, respectively. The wind attenuation factor is then

$$f_{\mathrm{wind}} = e^{-\tau_0} \gtrsim a^{-1} \xi_0^{-n}\,, \tag{B9}$$

where we have assumed $a\xi_0^n \gg 1$.

First consider the case of a thick disk which is not in the shadow of the inner attenuation zone of the corona. Unless the luminosity is so low that the corona is transparent (eq. [2.28]), this requires

$$\phi_{d\mathrm{IC}}\, \xi^s \gtrsim 0.1 \left(\frac{L}{k_\tau L_{\mathrm{E}}}\, \frac{T_{\mathrm{IC8}}}{\Xi_{h,\min}'\, \epsilon_{-1}}\right)^{1/4} > 0.03 \left(\frac{T_{\mathrm{IC8}}}{\Xi_{h,\min}'\, \epsilon_{-1}}\right)^{1/4} \tag{B10}$$

(cf. eqs. [2.23], [2.25], and discussion following [2.24]). With $f_{sh} = 1$ and $\phi_{dIC} > 0.02$, equations (B4), (B8), and (B9) yield

$$f_{wind} \gtrsim s\Xi'_0 T_{IC8}^{1/2} \left[2.5 \left(\frac{\xi_0 L_{cr}}{L} \right)^{2/3}, 1.6 \left(\frac{\xi_0 L_{cr}}{L} \right)^{1/3}, 0.6 \left(\frac{L_{cr}}{L} \right) \right] . \quad \text{(B11)}$$

For this unshadowed case we expect $s > 0.1$, so generally $f_{wind} \gtrsim 0.1$ as well.

In the opposite case the disk is thin and lies in the inner shadowed zone:

$$f_{wind}(\text{shadow}) \approx \frac{1.3}{T_{IC8}^{1/2}} \left(\frac{\phi_{dIC}}{10^{-2}} \right)^{1/2} \left(\frac{L}{L_{cr}} \right)^{1/4} f_{wind}(\text{no shadow}) . \quad \text{(B12)}$$

The total attenuation in this case is $f_{is} f_{wind}$(shadow). For binary X-ray sources, ϕ_{dIC} probably exceeds 10^{-2} (see Shakura and Sunyaev 1973); for quasars, the value is uncertain because of self-gravity in the disk.

REFERENCES

Angel, J. R. P. 1969, *Ap. J.*, **158**, 219.
Angel, J. R. P., and Stockman, H. S. 1980, *Ann. Rev. Astr. Ap.*, **18**, 321.
Begelman, M. C., McKee, C. F., and Shields, G. A. 1983, *Ap. J.*, **271**, 70 (Paper I).
Blandford, R., and McKee, C. F. 1982, *Ap. J.*, **255**, 419.
Blandford, R., and Payne, D. 1982, *M.N.R.A.S.*, **199**, 883.
Blandford, R., and Rees, M. 1978, in *Pittsburgh Conference on BL Lac Objects*, ed. A. M. Wolfe (Pittsburgh: University of Pittsburgh), p. 328.
Capriotti, E. R., Foltz, C., and Byard, P. 1980, *Ap. J.*, **241**, 903.
Chandrasekhar, S. 1960, *Radiative Transfer* (New York: Dover).
Charles, P. A., Thorstensen, J., and Barr, P. 1980, *Ap. J.*, **241**, 1148.
Chiappetti, L., Maraschi, L., Tanzi, E. G., and Treves, A. 1983, *Ap. J.*, **265**, 354.
Córdova, F. A., Mason, K. O., and Nelson, J. E. 1981, *Ap. J.*, **245**, 609.
Cowley, A. P., and Crampton, D. 1975, *Ap. J.* (*Letters*), **201**, L65.
Cowley, A. P., Crampton, D., and Hutchings, J. B. 1979, *Ap. J.*, **231**, 539.
———. 1982, *Ap. J.*, **255**, 596.
Crampton, D., Cowley, A. P., Hutchings, J. B., and Kaat, C. 1976, *Ap. J.*, **207**, 907.
Cunningham, C. 1976, *Ap. J.*, **208**, 534.
Fabian, A. C., Guilbert, P. W., and Ross, R. R. 1982, *M.N.R.A.S.*, **199**, 1045.
Flannery, B. P. 1975, *M.N.R.A.S.*, **170**, 325.
Holt, S. S., and McCray, R. 1982, *Ann. Rev. Astr. Ap.*, **20**, 323.
Jones, B. C., and Raine, D. J. 1980, *Astr. Ap.*, **81**, 128.
Kolykhalov, P. I., and Sunyaev, R. A. 1982, *Soviet Astr. Letters*, in press.
Krolik, J. H., McKee, C. F., and Tarter, C. B. 1981, *Ap. J.*, **249**, 422 (KMT).
Kwan, J., and Krolik, J. H. 1981, *Ap. J.*, **250**, 478.
Liang, E. P. T., and Price, R. H. 1977, *Ap. J.*, **218**, 247.
Liang, E. P. T., and Thompson, K. 1979, *M.N.R.A.S.*, **189**, 421.
Lightman, A. P., and Shapiro, S. L. 1975, *Ap. J.* (*Letters*), **198**, L73.
———. 1976, *Ap. J.*, **203**, 701.
London, R., McCray, R., and Auer, L. 1981, *Ap. J.*, **243**, 970.
Long, K., Chanan, G., and Novick, R. 1980, *Ap. J.*, **238**, 710.
Lynden-Bell, D. 1969, *Nature*, **233**, 690.
Mason, K. O., and Córdova, F. A. 1982*a*, *Ap. J.*, **255**, 603.
———. 1982*b*, *Ap. J.*, **262**, 253.
Mathews, W. G. 1982, *Ap. J.*, **258**, 425.
Mathews, W. G., Blumenthal, G. R., and Grandi, S. A. 1980, *Ap. J.*, **235**, 971.
McClintock, J. E., London, R., Bond, H., and Grauer, A. 1982, *Ap. J.*, **258**, 245.
McClintock, J. E., Remillard, R. A., and Margon, B. 1981, *Ap. J.*, **243**, 900.
Oke, J. B., and Korycansky, D. G. 1982, *Ap. J.*, **255**, 11.
Pacharintanakul, P., and Katz, J. I. 1980, *Ap. J.*, **238**, 985.
Paczyński, B. 1978, *Acta Astr.*, **28**, 91.
Parsignault, D. R., and Grindlay, J. E. 1978, *Ap. J.*, **225**, 970.
Payne, D. G., and Eardley, D. M. 1977, *Ap. Letters*, **19**, 39.
Rees, M. J. 1975, *M.N.R.A.S.*, **171**, 457.
Rees, M. J., Begelman, M. C., and Blandford, R. D. 1981, *Proceedings of Tenth Texas Symposium on Relativistic Astrophysics*, ed. R. Ramaty and F. C. Jones (New York: New York Academy of Science), p. 254.
Sakimoto, P. J., and Coroniti, F. V. 1981, *Ap. J.*, **247**, 19.
Schwarzenberg-Czerny, A. 1982, *Acta Astr.*, in press.
Shakura, N. I., and Sunyaev, R. A. 1973, *Astr. Ap.*, **24**, 337.
Shields, G. A. 1978, in *Pittsburgh Conference on BL Lac Objects*, ed. A. M. Wolfe (Pittsburgh: University of Pittsburgh), p. 257.
Shields, G. A., and McKee, C. F. 1981, *Ap. J.* (*Letters*), **246**, L57.
Stockman, H. S., and Angel, J. R. P. 1978, *Ap. J.* (*Letters*), **220**, L67.
Stockman, H. S., Angel, J. R. P., and Miley, G. K. 1979, *Ap. J.* (*Letters*), **227**, L55.
Thorstensen, J., Charles, P., Bowyer, S., Briel, U. G., Doxsey, R. E., Griffiths, R. E., and Schwartz, D. A. 1979, *Ap. J.* (*Letters*), **233**, L57.
White, N. E., Becker, R. H., Boldt, E. A., Holt, S. S., Serlemitsos, P. J., and Swank, J. H. 1981, *Ap. J.*, **247**, 994.
White, N. E., and Holt, S. S. 1982, *Ap. J.*, **257**, 318.
Williams, R. E. 1980, *Ap. J.*, **235**, 939.
Zel'dovich, Ya. B., and Pikel'ner, S. B. 1969, *Soviet Phys.—JETP*, **29**, 170.

M. BEGELMAN: Joint Institute for Laboratory Astrophysics, University of Colorado, Boulder, CO 80309

C. F. McKEE: Department of Physics, University of California, Berkeley, CA 94720